Excitons and optical nonlinearities in hybrid organic-inorganic nanostructures

1998 J. Phys.: Condens. Matter 10 9369

(http://iopscience.iop.org/0953-8984/10/42/005)

J. Phys.: Condens. Matter **10** (1998) 9369–9400. Printed in the UK PII: S0953-8984(98)82097-3

REVIEW ARTICLE

Excitons and optical nonlinearities in hybrid organic–inorganic nanostructures

V M Agranovich†, D M Basko‡, G C La Rocca‡ and F Bassani‡

† Institute for Spectroscopy, Russian Academy of Sciences, Troitsk, Moscow District, 142092, Russia

‡ Scuola Normale Superiore and INFM Piazza dei Cavalieri, I-56126 Pisa, Italy

Received 6 July 1998

Abstract. We present a theoretical review of the properties of electronic excitations in nanostructures based on combinations of organic materials with inorganic semiconductors, having respectively Frenkel excitons and Wannier–Mott excitons with nearly equal energies. We show that in this case the resonant coupling between organic and inorganic quantum wells (or wires or dots) may lead to several interesting effects, such as splitting of the excitonic spectrum and enhancement of the resonant optical nonlinearities.

First, we discuss the properties of hybrid Frenkel–Wannier–Mott excitons, which appear when the energy splitting of the excitonic spectrum is large compared to the width of the exciton resonances (the case of strong resonant coupling). Such peculiar excitations share at the same time both the properties of the Wannier excitons (e.g., the large radius) and those of the Frenkel excitons (e.g., the large oscillator strength). We discuss mainly two-dimensional configurations (interfaces or coupled quantum wells) which are the most extensively studied. In particular, we show that hybrid excitons are expected to have resonant optical nonlinearities significantly enhanced with respect to those of traditional inorganic or organic systems. We also consider analogous phenomena in microcavities where the exciton resonances are close to the cavity photon mode resonance.

Next, we consider the case of weak resonant coupling and show the relevance of the Förster mechanism of energy transfer from an inorganic quantum well to an organic overlayer. Such an effect may be especially interesting for applications: the electrical pumping of excitons in the semiconductor quantum well can be used to efficiently turn on the organic material luminescence.

1. Introduction

The need for systems having better optoelectronic properties to be used in applications has been driving researchers in materials science to develop novel compounds and novel structures. The progress in the field has been impressive, mainly due to the use of innovative growth techniques such as molecular beam epitaxy (MBE) and the realization of systems in two-dimensional (2D), one-dimensional (1D) and zero-dimensional (0D) confined geometries. We have now many newly developed organic or inorganic structures with very interesting properties. We mention here as a typical example the quest for efficient second-harmonic generation (SHG) where we can see a very peculiar 'competition' in the use of organic or inorganic materials. Inorganic semiconductors (e.g., GaAlAs, ZnCdSe) have been used to design MBE asymmetric quantum wells (QWs) having values of $\chi^{(2)}$ much larger than those of the corresponding bulk materials. Organic materials have also been used for the same purpose: molecular charge-transfer excitations lead to a strong enhancement of

0953-8984/98/429369+32$19.50

SHG. From the theoretical point of view, scientists working independently with covalent or molecular crystals have exploited actually the same basic idea, i.e. achieving a large change of static dipole moment upon excitation. In the present paper, we discuss the possibility of obtaining qualitatively new physical effects, potentially useful also for technological applications, by ingeniously combining organic with inorganic materials in one and the same hybrid structure.

The electronic excitations known as excitons play a fundamental role in the optical properties of dielectric solids [1]. They correspond to a bound state of one electron and one hole and can be created by light or can appear as a result of relaxation processes of free electrons and holes, which, for example, may be injected electrically. There are two models conventionally used to classify excitons—the small-radius Frenkel exciton model and the large-radius Wannier–Mott exciton model. The internal structure of Wannier–Mott excitons can be represented by hydrogen-like wavefunctions. Such a representation results from the two-particle, Coulombic electron–hole states in a crystalline periodic potential. The mean electron–hole distance for this type of exciton is typically large (in comparison with the lattice constant). On the other hand, the Frenkel exciton is represented as an electronic state of a crystal in which electrons and holes are placed on the same molecule. We can say that Frenkel excitons in organic crystals have radii a_F, comparable to the lattice constant: $a_F \sim a \sim 5$ Å. In contrast, weakly bound Wannier excitons in semiconductor QWs have large Bohr radii ($a_B \sim 100$ Å in III–V materials and $a_B \sim 30$ Å in II–VI ones; in both cases $a_B \gg a$). The oscillator strength of a Frenkel exciton is close to a molecular oscillator strength F, whereas the oscillator strength f of a Wannier exciton is usually much weaker: in a quantum well $f \sim a^3 a_B^{-2} L^{-1} F$ where L is the QW width ($a_B > L > a$). Both types of exciton interact with lattice vibrations through exciton–phonon coupling.

One of the main topics of our review is the optical nonlinearity due to exciton resonances. In high-quality semiconductors as well as in organic crystalline materials, the optical properties near and below the band gap are dominated by the exciton transitions and this is also the case for organic and inorganic QWs (or wires or dots). The excitonic optical nonlinearities in semiconductor QWs can be large because the ideal-bosonic approximation for Wannier excitons breaks down as soon as they start to overlap with each other, i.e., when their 2D density n becomes comparable to the saturation density $n_S \sim 1/(\pi a_B^2)$ (n_S is, typically, 10^{12} cm^{-2}). Then, due to phase-space filling (PSF), exchange and collisional broadening, the exciton resonance is bleached. However, a generic figure of merit for the optical nonlinearities scales like $I_P^{-1}(\Delta\chi/\chi)$ where $\Delta\chi$ is the nonlinear change in the susceptibility in the presence of a pump of intensity I_P. As $\Delta\chi/\chi \sim n/n_S \sim n a_B^2$, but also $n \propto f I_P \propto a_B^{-2} I_P$, such a figure of merit is nearly independent of the exciton Bohr radius [2]. As for the Frenkel excitons in organic crystals, simply because they have small radii, they have very large saturation density. Thus, pronounced PSF nonlinearities of the exciton resonance in molecular crystals are practically impossible to achieve as very high excitonic concentrations are needed. Of course, other mechanisms may effectively enhance the optical nonlinearities of organic materials, but their discussion falls outside the scope of this review.

Here we will consider hybrid structures in which Frenkel and Wannier excitons are in resonance with each other and coupled through their dipole–dipole interaction at the interface and through cavity photons in a microcavity. The basic idea is to realize the formation of new eigenstates given by appropriate coherent linear combinations of large-radius exciton states in the inorganic material and small-radius exciton states in the organic

one. We can expect that these hybrid electronic excitations will be characterized by a radius dominated by their Wannier component and by an oscillator strength dominated by their Frenkel component. Thus, they can have at the same time a large oscillator strength F and a small saturation density n_S. In this way, the desirable properties of both the inorganic and organic material unite and overcome the basic limitation mentioned above for the figure of merit of the exciton resonance nonlinearities. One of the most natural choices for implementing this idea is a layered structure with an interface between a covalent semiconductor and a crystalline molecular semiconductor. In such heterojunctions, there is obviously some cause for concern about the detrimental effects that lack of material purity and structural quality would have on the formation and the functional properties of the hybrid excitons. The realistic possibility of considering such organic–inorganic crystalline structures has only recently arisen due to progress in the development of the organic molecular beam deposition (OMBD) and other related techniques. Such progress has led to a monolayer-level control in the growth of organic thin films and superlattices with extremely high chemical purity and structural precision. This opens up a wide range of possibilities in the creation of a new type of ordered organic multilayer structure including highly ordered interfaces. It is well known that the requirement of lattice matching places strong restrictions on the materials which can be employed to produce high-quality interfaces using inorganic semiconductor materials. This is due to the fact that they are bonded by short-range covalent or ionic forces. In contrast, organic materials are bonded by weak van der Waals forces. This lifts such restrictions and broadens the choice of materials that can be used to prepare organic crystalline layered structures with the required properties (for more details and many examples, see reference [3]). In the following sections, we will discuss at length the electronic excitation spectra arising from the Frenkel–Wannier exciton hybridization in different geometrical configurations: quantum wells, quantum wires and quantum dots. At the same time, the nonlinear optical properties of hybrid excitons will be considered in detail: we predict a large enhancement of the excitonic resonant nonlinearities, in some cases of two orders of magnitude compared to those of traditional systems. A few other results on the physics of hybrid excitons taken from the current literature will also be presented.

We also consider the resonant interaction between Frenkel excitons in the organic QW and Wannier–Mott excitons in semiconductor QW in a microcavity where organic and inorganic QWs are separated. In this case the resonant interaction appears mainly through the cavity photons and can be very strong if the cut-off frequency of the cavity photon is close to the excitonic resonances. We demonstrate that in this case new hybrid Frenkel–Wannier–Mott exciton–cavity photon states can be tailored to engineer the fluorescence efficiency and relaxation processes.

In all of the cases mentioned above, we have assumed that the resonance splitting in the exciton spectra is large in comparison with the relaxation width of the resonances (the strong-coupling regime). However, for organic materials in many instances the width of the excitonic resonances can be larger than possible frequency shifts or splitting. In such a situation (the weak-coupling regime), instead of a coherent superposition of excitonic states, the Förster energy transfer from the inorganic QW to the organic QW has to be considered. We investigate this phenomenon in detail, considering the energy transfer to organics from free and localized Wannier–Mott excitons as well as from unbound electron–hole pairs. We show that this can produce efficient luminescence in the organic layers with electrical current pumping of the inorganic material.

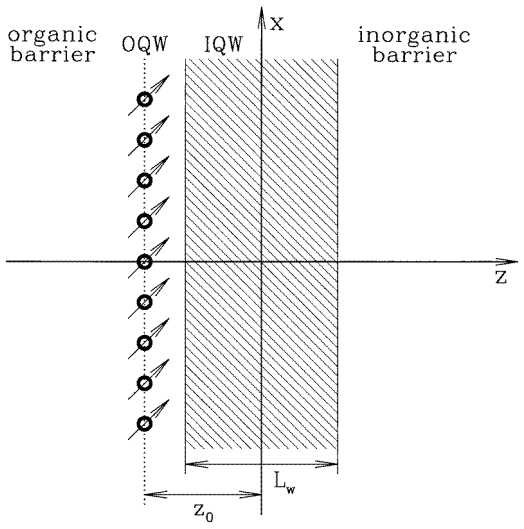

Figure 1. The physical configuration under study.

2. 2D hybrid excitons

2.1. Electronic states and linear optics

Here we study the dipole–dipole interaction between an organic quantum well (OQW) and an inorganic one (IQW) and demonstrate how new hybrid states arise [4]. The configuration that we consider is the following. A plane semiconductor IQW of thickness L_w occupies the region $|z| < L_w/2$, the z-axis being chosen to lie along the growth direction. All of the space with $z > L_w/2$ is filled by the barrier material and that with $z < -L_w/2$ by the organic material in which the OQW is placed (figure 1). For simplicity, we treat the organic molecules in the dipole approximation, neglecting the contribution of higher multipoles to the interaction, and we consider the OQW as a single monolayer, i.e., as a 2D lattice of molecules at discrete sites $\boldsymbol{n}$, placed at $z = -z_0 < -L_w/2$ (the generalization to the case of several monolayers is easy). All of the semiconductor well–barrier structure ($z > -L_w/2$) is assumed to have the same background dielectric constant ε, while the organic half-space ($z < -L_w/2$) is taken to have the dielectric constant $\tilde{\varepsilon}$ (corresponding to the organic substrate).

Due to the difference in electronic structure of the two QWs under consideration, one may neglect the single-particle wavefunction mixing; in other words, the OQW and the IQW states are assumed to have zero wavefunction overlap. Assuming a perfect 2D translational invariance of the system, we classify the excitons according to their in-plane wavevector $\boldsymbol{k}$. Suppose that for some bands of Frenkel excitons in the OQW and Wannier–Mott excitons in the IQW the energy separation is much less than the distance to other exciton bands. Then we take into account only the mixing between these two bands. We choose as a basis set the 'pure' Frenkel and Wannier states, i.e., the state in which the OQW is excited, while the IQW is in its ground state (denoted by $|F, \boldsymbol{k}\rangle$), and vice versa (denoted by $|W, \boldsymbol{k}\rangle$), their energies being $E_F(\boldsymbol{k})$ and $E_W(\boldsymbol{k})$. We seek the new hybrid states in the form

$$|\alpha, \boldsymbol{k}\rangle = A_\alpha(\boldsymbol{k})|F, \boldsymbol{k}\rangle + B_\alpha(\boldsymbol{k})|W, \boldsymbol{k}\rangle \tag{1}$$

where $\alpha =$ 'u', 'l' labels the two resulting states (upper and lower branches). The

Schrödinger equation for the coefficients A, B is then written as

$$\begin{aligned}(E_F(\boldsymbol{k}) - E)A(\boldsymbol{k}) + \langle F, \boldsymbol{k}|\hat{H}_{int}|W, \boldsymbol{k}\rangle B(\boldsymbol{k}) = 0\\ \langle W, \boldsymbol{k}|\hat{H}_{int}|F, \boldsymbol{k}\rangle A(\boldsymbol{k}) + (E_W(\boldsymbol{k}) - E)B(\boldsymbol{k}) = 0\end{aligned} \tag{2}$$

where $\hat{H}_{int}$ is the Hamiltonian of the dipole–dipole interaction between the QWs. Solution of (2) gives the energies of the upper and lower branches and the splitting $\Delta(\boldsymbol{k})$:

$$E_{u,l}(\boldsymbol{k}) = \frac{E_F(\boldsymbol{k}) + E_W(\boldsymbol{k}) \pm \Delta(\boldsymbol{k})}{2} \qquad \Delta(\boldsymbol{k}) \equiv \sqrt{(E_F(\boldsymbol{k}) - E_W(\boldsymbol{k}))^2 + 4\Gamma^2(\boldsymbol{k})} \tag{3}$$

where we use the notation $\Gamma(\boldsymbol{k}) \equiv |\langle W, \boldsymbol{k}|\hat{H}_{int}|F, \boldsymbol{k}\rangle|$ for the coupling matrix element. For the orthonormalized new states the weighting coefficients are given by

$$|A_u(\boldsymbol{k})|^2 = |B_l(\boldsymbol{k})|^2 = \frac{1}{2}\left(1 + \frac{E_F(\boldsymbol{k}) - E_W(\boldsymbol{k})}{\Delta(\boldsymbol{k})}\right) \tag{4}$$

$$|A_l(\boldsymbol{k})|^2 = |B_u(\boldsymbol{k})|^2 = \frac{1}{2}\left(1 - \frac{E_F(\boldsymbol{k}) - E_W(\boldsymbol{k})}{\Delta(\boldsymbol{k})}\right). \tag{5}$$

To evaluate the matrix element $\Gamma_{\boldsymbol{k}}$ we write the interaction Hamiltonian as

$$\hat{H}_{int} = -\sum_{\boldsymbol{n}} \hat{\boldsymbol{p}}^F(\boldsymbol{n}) \cdot \hat{\boldsymbol{\mathcal{E}}}(\boldsymbol{n}) \tag{6}$$

where $\hat{\boldsymbol{p}}^F(\boldsymbol{n})$ is the operator of the dipole moment of the organic molecule situated at the lattice site $\boldsymbol{n}$, and $\hat{\boldsymbol{\mathcal{E}}}(\boldsymbol{n})$ is the operator of the electric field at the point $\boldsymbol{n}$, produced by the IQW exciton. If we introduce the operator of the IQW polarization $\hat{\boldsymbol{P}}^W(\boldsymbol{r})$, then the operators $\hat{\boldsymbol{\mathcal{E}}}(\boldsymbol{n})$ and $\hat{\boldsymbol{P}}^W(\boldsymbol{r})$ are related to each other in exactly the same way as the corresponding classical quantities in electrostatics:

$$\hat{\mathcal{E}}_i(\boldsymbol{r}) = \int \mathrm{d}^3\boldsymbol{r}'\ \mathcal{D}_{ij}(\boldsymbol{r}_\parallel - \boldsymbol{r}'_\parallel, z, z')\hat{P}^W_j(\boldsymbol{r}') \tag{7}$$

where $i, j = x, y, z$, $\boldsymbol{r}_\parallel \equiv (x, y)$ and $\mathcal{D}_{ij}(\boldsymbol{r}, \boldsymbol{r}')$ is the Green's function appearing in the analogous problem of classical electrostatics. It is equal to the ith Cartesian component of the classical static electric field at the point $\boldsymbol{r}$, produced by the jth component of the classical point dipole, situated at the point $\boldsymbol{r}'$ and is connected to the Green's function G of the Poisson equation in an inhomogeneous medium with the dielectric constant $\varepsilon_{ij}(\boldsymbol{r})$:

$$\mathcal{D}_{ij}(\boldsymbol{r}, \boldsymbol{r}') = -\frac{\partial}{\partial x_i}\frac{\partial}{\partial x'_j}G(\boldsymbol{r}, \boldsymbol{r}') \tag{8}$$

$$\frac{\partial}{\partial x_i}\varepsilon_{ij}(\boldsymbol{r})\frac{\partial}{\partial x_j}G(\boldsymbol{r}, \boldsymbol{r}') = -4\pi\delta(\boldsymbol{r} - \boldsymbol{r}'). \tag{9}$$

Since our system is translationally invariant in two dimensions, it is convenient to consider the Fourier transform:

$$\mathcal{D}_{ij}(\boldsymbol{r}_\parallel - \boldsymbol{r}'_\parallel, z, z') = \int \frac{\mathrm{d}^2\boldsymbol{k}}{(2\pi)^2}\ \mathcal{D}_{ij}(\boldsymbol{k}, z, z')\mathrm{e}^{\mathrm{i}\boldsymbol{k}\cdot(\boldsymbol{r}_\parallel - \boldsymbol{r}'_\parallel)} \tag{10}$$

and analogously for $G(\boldsymbol{r}_\parallel - \boldsymbol{r}'_\parallel, z, z')$. Then $G(\boldsymbol{k}, z, z')\mathrm{e}^{\mathrm{i}\boldsymbol{k}\cdot\boldsymbol{r}_\parallel}$ is the potential, produced by a charge-density wave $\rho(\boldsymbol{r}) = \delta(z - z')\mathrm{e}^{\mathrm{i}\boldsymbol{k}\cdot\boldsymbol{r}_\parallel}$. In our case the dielectric constant is a simple step function

$$\varepsilon_{ij}(\boldsymbol{r}) = \begin{cases}\tilde{\varepsilon}\delta_{ij} & z < -L_w/2\\ \varepsilon\delta_{ij} & z > -L_w/2\end{cases} \tag{11}$$

and the potential may be readily found from Poisson's equation

$$\left(\frac{\mathrm{d}^2}{\mathrm{d}z^2} - k^2\right) G(\boldsymbol{k}, z, z') = -\frac{4\pi\delta(z - z')}{\varepsilon(z)} \tag{12}$$

with the usual electrostatic boundary conditions at the interface $z = -L_w/2$ (continuity of the tangential component of the electric field $-\mathrm{i}\boldsymbol{k}G$ and of the normal component of the electric displacement $-\varepsilon(z)\,\partial G/\partial z$). The Green's function $\mathcal{D}_{ij}$ for $z < -L_w/2$, $z' > -L_w/2$ is then given by

$$\mathcal{D}_{ij}(\boldsymbol{k}, z, z') = \frac{4\pi}{\varepsilon + \tilde{\varepsilon}} k \mathrm{e}^{k(z-z')} \left(\frac{\mathrm{i}k_i}{k} + \delta_{i,z}\right)\left(\frac{\mathrm{i}k_j}{k} + \delta_{j,z}\right). \tag{13}$$

Thus, the matrix element of $\hat{H}_{int}$ that we are interested in can be written as

$$\langle F, \boldsymbol{k}|\hat{H}_{int}|W, \boldsymbol{k}\rangle = -\sum_{\boldsymbol{n}} \int \mathrm{d}^3\boldsymbol{r}\ \langle F, \boldsymbol{k}|\hat{p}_i(\boldsymbol{n})|0\rangle \mathcal{D}_{ij}(\boldsymbol{n} - \boldsymbol{r}_\parallel, -z_0, z)\langle 0|\hat{P}_j^W(\boldsymbol{r})|W, \boldsymbol{k}\rangle. \tag{14}$$

The matrix element of the IQW polarization between the ground state $|0\rangle$ and $|W, \boldsymbol{k}\rangle$ for the 1s exciton with Bohr radius a_B is equal to [5, 6]

$$\langle 0|\hat{\boldsymbol{P}}^W(\boldsymbol{r})|W, \boldsymbol{k}\rangle = \sqrt{\frac{2}{\pi}} \frac{\boldsymbol{d}^{vc}}{a_B} \frac{\mathrm{e}^{\mathrm{i}\boldsymbol{k}\cdot\boldsymbol{r}_\parallel}}{\sqrt{S}} \chi^e(z)\chi^h(z) \tag{15}$$

where $\sqrt{2/(\pi a_B^2)}$ is the value of the 1s wavefunction of the relative motion of the electron and hole, taken at $r_\parallel = 0$; $\chi^e(z)$, $\chi^h(z)$ are the envelope functions for the electron and hole in the IQW confinement potential (we assume the IQW to be thin, so that the transverse and the relative in-plane motion of the electron and hole are decoupled) and S is the in-plane normalization area. Finally,

$$\boldsymbol{d}^{vc} = \int_{uc} u_v^*(\boldsymbol{r})(-e\boldsymbol{r})u_c(\boldsymbol{r})\ \mathrm{d}^3\boldsymbol{r} \tag{16}$$

is the matrix element of the electric dipole moment connecting the conduction and valence bands ($\boldsymbol{d}^{vc}$ is taken to be independent of $\boldsymbol{k}$, $u_{c\,(v)}$ are the Bloch functions for the conduction (valence) band extremum and the integration in (16) is performed over the unit cell). Its Cartesian components d_i^{vc} ($i = x, y, z$) may be expressed in terms of the Kane energy E_0 [5]:

$$|d_i^{vc}|^2 = \frac{e^2\hbar^2 E_0 c_i^2}{2m_0 E_g^2} \tag{17}$$

where m_0 is the free-electron mass, E_g is the energy gap between the conduction and valence bands and c_i is the appropriate symmetry coefficient. In semiconductors with the zinc-blende structure, $c_x^{hh} = c_y^{hh} = 1/\sqrt{2}$, $c_z^{hh} = 0$ (heavy holes) and $c_x^{lh} = c_y^{lh} = 1/\sqrt{6}$, $c_z^{lh} = \sqrt{(2/3)}$ (light holes). We see that only light holes can contribute to the z-component of the IQW polarization.

For the Frenkel exciton the dipole moment matrix element, contributing to the matrix element (14), is given by

$$\langle F, \boldsymbol{k}|\hat{p}_i(\boldsymbol{n})|0\rangle = \frac{\mathrm{e}^{-\mathrm{i}\boldsymbol{k}\cdot\boldsymbol{n}}}{\sqrt{N}} \boldsymbol{d}^{F*} = \frac{\mathrm{e}^{-\mathrm{i}\boldsymbol{k}\cdot\boldsymbol{n}}}{\sqrt{S}} a_F \boldsymbol{d}^{F*} \tag{18}$$

where $\boldsymbol{d}^F$ is the transition dipole moment for a single organic molecule (analogous to $\boldsymbol{d}^{vc}$ for the semiconductor), N is the total number of sites in the lattice and a_F is the lattice constant, which may be considered as the radius of the Frenkel exciton.

Now we can write out the final expression for the coupling matrix element:

$$\langle F, \boldsymbol{k}|\hat{H}_{int}|W, \boldsymbol{k}\rangle = -\sqrt{\frac{2}{\pi}}\frac{d_i^{F*}}{a_F}\frac{d_j^{vc}}{a_B}\int \mathrm{d}z\ \mathcal{D}_{ij}(\boldsymbol{k}, -z_0, z)\chi^e(z)\chi^h(z). \tag{19}$$

From equations (13), (19) we see that the only contributing polarizations for the semiconductor are those along $\boldsymbol{k}$ (L-modes) and along the growth direction $\boldsymbol{z}$ (Z-modes, only for the light holes, according to equation (17)). For simplicity we take the electron and hole confinement wavefunctions for the lowest subbands in the approximation of an infinitely deep IQW:

$$\chi^e(z)\chi^h(z) = \frac{2}{L_w}\cos^2\left(\frac{\pi z}{L_w}\right) \tag{20}$$

and assume the transition dipole moment in the organics $\boldsymbol{d}^F$ to be real (which is always possible with an appropriate choice of molecular wavefunctions). Without loss of generality we may take the vector $\boldsymbol{k}$ along the x-axis. Evaluating the integral in (19), we obtain the interaction parameter $\Gamma_{L,Z}$ for the L- and Z-modes:

$$\Gamma_{L\,(Z)}(k) = \frac{8\sqrt{2\pi}}{\varepsilon+\tilde{\varepsilon}}\frac{\mathrm{e}^{-kz_0}\sinh(kL_w/2)}{1+(kL_w/2\pi)^2}\frac{|d^{vc}_{x(z)}|\sqrt{(d_x^F)^2+(d_z^F)^2}}{a_F a_B L_w}. \tag{21}$$

It is seen that $\Gamma(k)$ has a maximum Γ_{max} at $k = k_{max}$. The value of k_{max} for arbitrary z_0 and L_w may be found numerically; for $z_0 - L_w/2 > 0.1L_w$ it is well described by the formula

$$k_{max} \simeq \frac{1}{L_w}\ln\left(\frac{2z_0+L_w}{2z_0-L_w}\right) \tag{22}$$

while in the limit $z_0 \simeq L_w/2$ we have $k_{max} \simeq 2.4/L_w$.

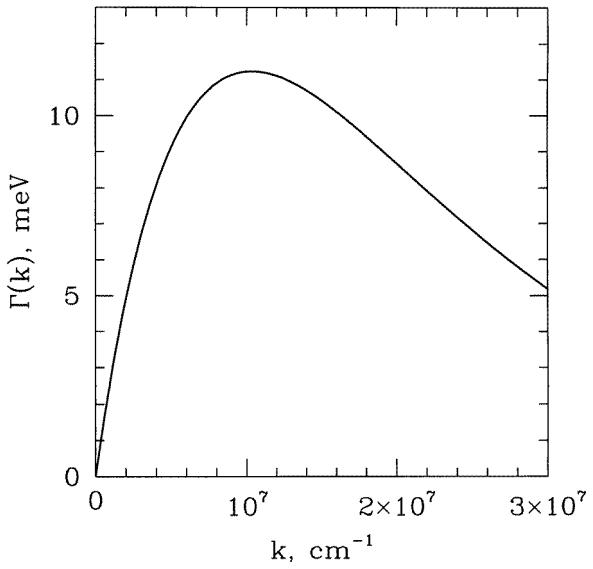

Figure 2. The interaction parameter $\Gamma(k)$ for $d^{vc} = 12$ D (D ≡ debye), $d^F = 5$ D, $a_B = 25$ Å, $a_F = 5$ Å, $L_w = 10$ Å, $z_0 = 10$ Å, $\varepsilon_\infty = 6$, $\tilde{\varepsilon}_\infty = 4$.

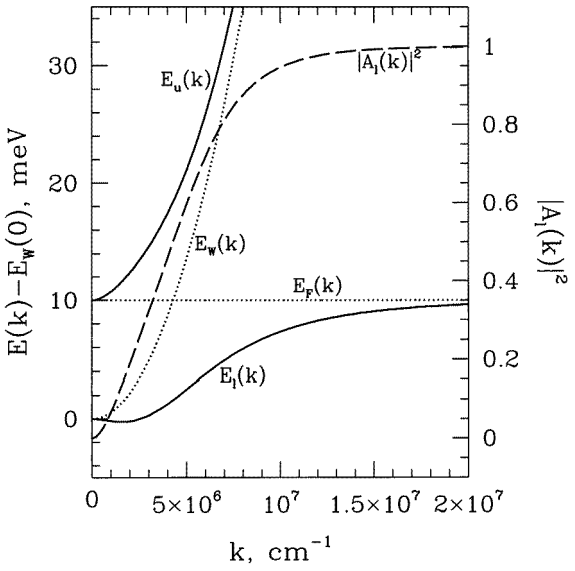

Figure 3. The dispersion $E_{u,l}(k)$ of the upper and lower hybrid exciton branches (solid lines) and that of the unperturbed Frenkel and Wannier excitons (dotted lines). The 'weight' of the FE component in the lower branch $|A_l(k)|^2$ is shown by the dashed line. The parameters are the same as in figure 2 ($m_W = 0.7m_0$); the detuning $\delta = 10$ meV.

We approximate the WE dispersion by a parabola with the in-plane effective mass $m_W = m_e + m_h$, $m_{e(h)}$ being the electron (hole) mass, and neglect the FE dispersion since the typical masses are (5–100)m_0:

$$E_W(\boldsymbol{k}) = E_W(0) + \frac{\hbar^2 k^2}{2m_W} \qquad E_F(\boldsymbol{k}) = E_F(0) \qquad E_F(0) - E_W(0) \equiv \delta. \tag{23}$$

We will measure all energies with respect to $E_W(0)$. The dispersion of the hybrid states (3) can be written as

$$E_{u,l}(\boldsymbol{k}) - E_W(0) = \frac{\delta}{2} + \frac{\hbar^2 k^2}{4m_W} \pm \sqrt{\left(\frac{\delta}{2} - \frac{\hbar^2 k^2}{4m_W}\right)^2 + \Gamma^2(\boldsymbol{k})}. \tag{24}$$

To obtain numerical estimates we choose the following values of parameters. For the IQW those representative of II–VI semiconductor (e.g., ZnSe/ZnCdSe) quantum wells are taken [7]: $\varepsilon = \varepsilon_\infty = 6$, $d^{vc}/a_B \approx 0.1e$ (which corresponds to $d^{vc} \simeq 12$ D and a Bohr radius of 25 Å), the exciton mass $m_W = 0.7m_0$ and the well width $L_w = 10$ Å. For the organic part of the structure, we take parameters typical of such media (e.g., see [3, 8, 9]): $\tilde{\varepsilon} = \tilde{\varepsilon}_\infty = 4$, the transition dipole for the molecules in the monolayer $d^F = 5$ D, $a_F = 5$ Å and $z_0 = 10$ Å. We plot $\Gamma(k)$ for these values of the parameters in figure 2. We see that $\Gamma_{max} \simeq 11$ meV. The dispersion curves $E_{u,l}(k)$ along with the FE weight in the lower branch $|A_l(k)|^2$ for three different detunings $\delta = 10$ meV, $\delta = 0$ and $\delta = -10$ meV are plotted in figures 3–5.

For $\delta > 0$ the properties of the excited states are changed drastically. In this case the zero-approximation dispersion curves for FE and WE cross at the point $k = k_0 = \sqrt{2m_W\delta/\hbar^2}$. At $k = 0$ the upper states are purely F-like and the lower states W-like; at $k \sim k_0$ they are strongly mixed and a large splitting of their dispersion curves is present,

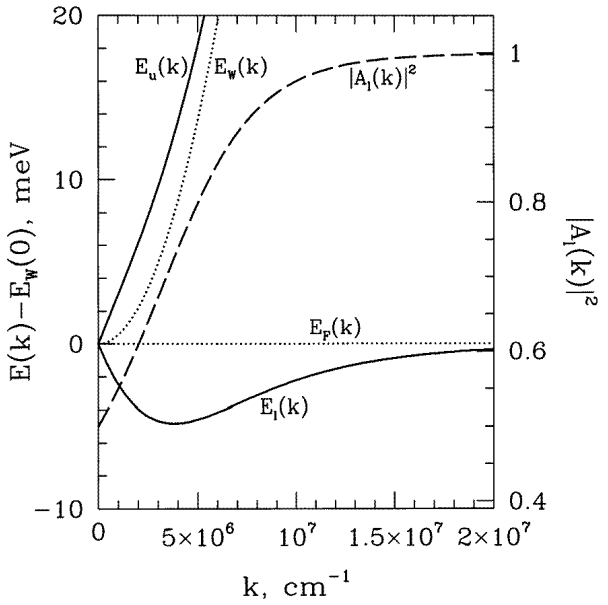

Figure 4. As figure 3, but for $\delta = 0$.

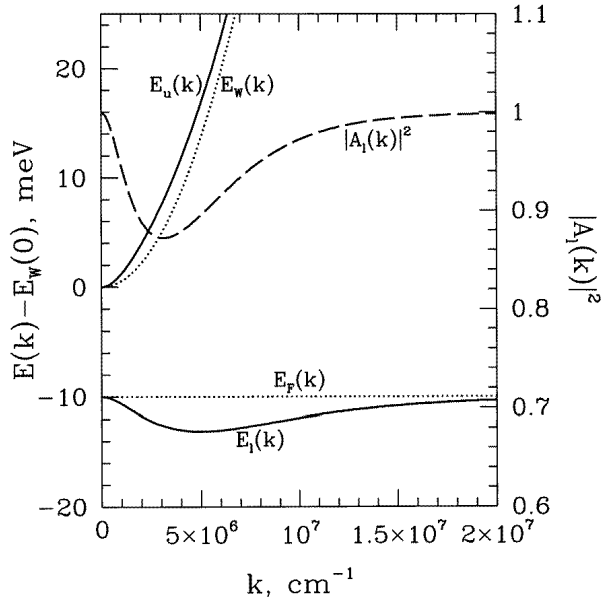

Figure 5. As figure 3, but for $\delta = -10$ meV.

$\Delta(k_0) \sim 2\Gamma(k_0)$, and for large k ($k \gg k_0$) they 'interchange': the upper branch becomes W-like with the quadratic dispersion and excitations of the lower branch tend to FE. If $\delta < 0$, then $E_W(k) > E_F(k)$ for all k and no crossing occurs; $E_u(k)$ closely follows the WE dispersion and $|A_u(k)|^2 \ll 1$; the lower state is FE-like.

A nontrivial feature of the lower-branch dispersion is a minimum away from $k = 0$, which is always present for $\delta \leqslant 0$ as well as for some positive values of δ, $0 < \delta < \delta_{cr}$, and is at its deepest for $\delta = 0$. The critical value of δ may be found if one looks at the

values of the derivatives of $E_l(k)$ at $k = 0$. It turns out that

$$\begin{aligned} &\frac{\mathrm{d}E_l(0)}{\mathrm{d}k} = 0 \qquad (\delta \neq 0) \\ &\frac{\mathrm{d}^2E_l(0)}{\mathrm{d}k^2} < 0 \qquad (\delta < \delta_{cr}) \\ &\frac{\mathrm{d}^2E_l(0)}{\mathrm{d}k^2} > 0 \qquad (\delta > \delta_{cr}) \end{aligned} \tag{25}$$

and δ_{cr} when the minimum 'splits' off $k = 0$ is given by

$$\delta_{cr} = \left(\frac{\mathrm{d}\Gamma(0)}{\mathrm{d}k}\right)^2 \frac{2m_W}{\hbar^2}. \tag{26}$$

For our parameters, $\delta_{cr} \simeq 16$ meV. For large negative values of $\delta \ll -\Gamma_{max}$, the lower-branch dispersion at $k \ll \sqrt{2m_W\delta/\hbar^2}$ may be approximated as

$$E_l(k) - E_W(0) \simeq -|\delta| - \frac{\Gamma^2(k)}{|\delta|}. \tag{27}$$

So, the depth of the minimum for large $|\delta|$ is $\Gamma^2_{max}/|\delta|$ while for small δ it is of the order of Γ_{max} and we see that effective range of δ when the minimum is the most pronounced is $-\Gamma_{max} \lesssim \delta < \delta_{cr}$. As a consequence, at low temperatures and under optical pumping at frequencies above the excitonic resonance, excitons will accumulate in this minimum, which can be detected, for example, by pump–probe experiments. The fluorescence from these states should increase with temperature, since states with small k become populated.

If an incident electromagnetic wave with the electric field $\boldsymbol{\mathcal{E}}(\boldsymbol{r}) = \boldsymbol{\mathcal{E}}_0 \mathrm{e}^{\mathrm{i}\boldsymbol{Q}\cdot\boldsymbol{r}}$ is present, then the interaction with the hybrid structure is described by the Hamiltonian (neglecting the local field corrections)

$$\hat{H}_{em} = -\boldsymbol{\mathcal{E}}_0 \cdot \left(\sum_{\boldsymbol{n}} \hat{\boldsymbol{p}}^F(\boldsymbol{n})\mathrm{e}^{\mathrm{i}\boldsymbol{Q}_\parallel\cdot\boldsymbol{n}} + \int \mathrm{d}z \int \mathrm{d}^2\boldsymbol{r}_\parallel \; \hat{\boldsymbol{P}}^W(\boldsymbol{r})\mathrm{e}^{\mathrm{i}\boldsymbol{Q}_\parallel\cdot\boldsymbol{r}_\parallel}\right) \tag{28}$$

where we have neglected the z-dependence of the incident field since the thickness of our structure is much less than the light wavelength. The corresponding matrix element is different from zero only if $\boldsymbol{k} = \boldsymbol{Q}_\parallel$ and in this case is equal to

$$\langle\alpha, \boldsymbol{k}|\hat{H}_{em}|0\rangle \equiv -\boldsymbol{\mathcal{E}}_0 \cdot \boldsymbol{M}^\alpha_{\boldsymbol{k}} = -\boldsymbol{\mathcal{E}}_0 \cdot \left(A^*_\alpha(\boldsymbol{k})\boldsymbol{M}^F + B^*_\alpha(\boldsymbol{k})\boldsymbol{M}^W_{\boldsymbol{k}}\right) \tag{29}$$

where

$$\boldsymbol{M}^F = \sqrt{N}\boldsymbol{d}^{F*} = \frac{\sqrt{S}}{a_F}\boldsymbol{d}^{F*} \tag{30}$$

$$\boldsymbol{M}^W_{\boldsymbol{k}} = \sqrt{\frac{2}{\pi}}\frac{\sqrt{S}}{a_B}\boldsymbol{d}^{vc*}\int \chi^{e*}(z)\chi^{h*}(z)\,\mathrm{d}z \tag{31}$$

are the optical matrix elements for the isolated OQW and IQW respectively, which are independent of $\boldsymbol{k}$. Usually we have $M^F \gg M^W$ since $a_F \ll a_B$, and in the region of strong mixing, the oscillator strength f^α of a hybrid state is determined by its FE component:

$$f^\alpha(\boldsymbol{k}) \simeq |A_\alpha(\boldsymbol{k})|^2 f^F. \tag{32}$$

At the crossing point $k = k_0$ (for $\delta > 0$) we have $|A_\alpha(k_0)|^2 = 1/2$ and the FE oscillator strength is equally distributed between the two hybrid states. For the hybrid exciton radii the opposite relation holds. Calculating the expectation value of the exciton radius squared $\hat{r}^2$ in the state $|\alpha, \boldsymbol{k}\rangle$ we obtain

$$\langle\alpha, \boldsymbol{k}|\hat{r}^2|\alpha, \boldsymbol{k}\rangle = |A_\alpha(\boldsymbol{k})|^2\langle F, \boldsymbol{k}|\hat{r}^2|F, \boldsymbol{k}\rangle + |B_\alpha(\boldsymbol{k})|^2\langle W, \boldsymbol{k}|\hat{r}^2|W, \boldsymbol{k}\rangle \simeq |B_\alpha(\boldsymbol{k})|^2 a_B^2 \tag{33}$$

since $a_B \gg a_F$ and we neglect the latter. Cross terms do not appear since we neglect the single-particle wavefunction mixing between the two QWs.

We see that the new states can possess both large oscillator strengths and large exciton radii. This effect is especially pronounced if the crossing of the FE and WE dispersion curves occurs for the value of the wavevector close to that of the maximum of the coupling strength: $k_0 \simeq k_{max}$. Since k_0 is determined by the detuning δ, and k_{max}, in turn, depends on L_w and z_0 (equation (22)), a special choice of these parameters should be made for maximizing the effect. Also, in order to take advantage of the hybrid states in optics, the wavevector of light in the medium $q = n_\infty \omega/c$ (n_∞ being the background refraction index) should not be far from k_0. Usually, near excitonic resonances, $q < k_0$ and special care should be taken to overcome this difficulty (e.g., using a coupled diffraction grating with period $2\pi/k_0$ [10] or a prism). We mention, however, that even in the region of small wavevectors in which the 2D excitons are radiative, the hybridization may be realized not due to the instantaneous dipole–dipole interaction, but due to the retarded interaction stemming from the exchange of photons. Such a situation has been analysed (even in the nonlinear regime) with an appropriate transfer-matrix approach, which is equivalent to the solution of the full Maxwell equations [11].

As regards the choice of materials for the implementation of the system considered here, examples of molecular substances having small-radius ($\leqslant 5$ Å) excitons with energies of a few eV, among those already successfully grown [3] as crystalline layers on a variety of inorganic (including semiconductor) crystals, are the acenes, such as tetracene (2 eV) or pentacene (1.5 eV), the metal phthalocyanines, such as VOPc (1.6 eV) or CuPc (1.8 eV), and the tetracarboxylic compounds, such as NTCDA (3.1 eV) or PTCDA (2.2 eV). Semiconductors having large-radius excitons with matching energies are, for instance, the III–V and II–VI ternary solid solutions such as GaAlAs, ZnCdSe and ZnSSe [12]; beside a judicious choice of alloy composition and well thickness, a fine tuning of the resonance condition could be achieved by applying an external static electric field along the growth direction (the quantum-confined Stark effect [13]; for hybrid excitons it has been considered in reference [14]). A major experimental problem is the control of the interface quality: the inhomogeneous broadening should remain small and the in-plane wavevector $\boldsymbol{k}$ a (sufficiently) good quantum number; organic superlattices with high-quality interfaces have been demonstrated [3]. The necessary condition for the hybrid states to be observable is that the exciton linewidths must be smaller than the splitting $\Delta(k)$. This is the case in the present calculations, where for $k_0 = k_{max}$ we have $\Delta(k_0) = 2\Gamma_{max} \simeq 20$ meV, while in inorganic QWs the homogeneous linewidth at low temperatures is $\sim$1 meV [15, 16]. The nonradiative linewidth of a 2D Frenkel exciton in an OQW can also be small: in the case of a 2D exciton in the external monolayer of anthracene, this linewidth at low temperatures is $\sim$2 meV [17]. In principle, apart from the resonance condition and the large difference in excitonic radii, the present model demands no specific requirements and the rapid progress in the growth of organic crystalline multilayers justifies some optimism about its concrete realization.

We also mention here the work of D'Andrea and Muzi [18], where the effects of the exciton–phonon interaction in hybrid systems were studied. In this work the resonant Raman spectroscopy is also suggested as a tool for studying hybrid organic–inorganic QWs.

2.2. Nonlinear optics

2.2.1. The resonant $\chi^{(3)}$-nonlinearity. From the results of the previous subsection we may expect that the exciton hybridization should strongly modify the nonlinear optical properties

of the structure under consideration. Indeed, hybrid excitons can combine both a large oscillator strength, which makes it easy to produce large populations, and a large radius, which, in turn, leads to low saturation densities. In this subsection we analyse the situation quantitatively [19], calculating the response of the interband polarization $\boldsymbol{P} = \boldsymbol{P}^W + \boldsymbol{P}^F$ to the external driving electric field (corresponding to a cw experiment)

$$\boldsymbol{\mathcal{E}}(\boldsymbol{r}, t) = \boldsymbol{\mathcal{E}}_0 \mathrm{e}^{\mathrm{i}\boldsymbol{Q}\cdot\boldsymbol{r} - \mathrm{i}\omega t} + \mathrm{CC} \tag{34}$$

in the presence of a large density of excitations using the standard technique of semiconductor Bloch equations [13, 20]. Since we are considering a cw experiment, the populations are stationary and may be treated as parameters in the equation for the time-dependent interband polarization.

First, we express the operator of the electron–hole interband polarization $\hat{\boldsymbol{P}}^W(\boldsymbol{r})$ in terms of the electron and hole creation and annihilation operators in the envelope function approximation, following the standard procedure [5, 20]:

$$\hat{\boldsymbol{P}}^W(\boldsymbol{r}) = \frac{\boldsymbol{d}^{vc}}{S} \chi^e(z)\chi^h(z) \sum_{\boldsymbol{k},\boldsymbol{q}} \mathrm{e}^{\mathrm{i}\boldsymbol{k}\cdot\boldsymbol{r}_\parallel} \hat{h}_{-\boldsymbol{q}} \hat{c}_{\boldsymbol{k}+\boldsymbol{q}} + \mathrm{HC}. \tag{35}$$

Here $\chi^e(z)$, $\chi^h(z)$ are electron and hole wavefunctions in the given IQW subbands (resonant with the FE), $\hat{c}_{\boldsymbol{k}}$ and $\hat{h}_{\boldsymbol{k}}$ are annihilation operators for an electron and hole with the in-plane wavevector $\boldsymbol{k}$ in the subbands under consideration, S is the in-plane normalization area and $\boldsymbol{d}^{vc}$ is the matrix element (16). We do not take into account the spin degeneracy, considering thus the polarization produced by electrons and holes with a given spin (thus, the final expression for the susceptibility should be multiplied by two). An analogous expression for the OQW polarization is

$$\hat{\boldsymbol{P}}^F(\boldsymbol{r}) = \frac{\boldsymbol{d}^F}{a_F\sqrt{S}} \delta(z + z_0) \sum_{\boldsymbol{k}} \mathrm{e}^{\mathrm{i}\boldsymbol{k}\cdot\boldsymbol{r}_\parallel} \hat{B}_{\boldsymbol{k}} + \mathrm{HC} \tag{36}$$

where $\hat{B}_{\boldsymbol{k}}$ is the annihilation operator for the Frenkel exciton, which is assumed to be tightly bound.

Besides the term of the Hamiltonian describing free Frenkel excitons and free electron–hole pairs (with the single-particle energies $E_F(\boldsymbol{k})$, $\varepsilon_e(\boldsymbol{k})$ and $\varepsilon_h(\boldsymbol{k})$ correspondingly), the Hamiltonian that we consider here includes the following.

(i) The Coulomb interaction between electrons and holes:

$$\hat{H}_{Coul} = \frac{1}{2S} \sum_{\boldsymbol{q}\neq 0} v(\boldsymbol{q}) \sum_{\boldsymbol{k},\boldsymbol{k}'} (\hat{c}^\dagger_{\boldsymbol{k}+\boldsymbol{q}} \hat{c}^\dagger_{\boldsymbol{k}'-\boldsymbol{q}} \hat{c}_{\boldsymbol{k}'} \hat{c}_{\boldsymbol{k}} + \hat{h}^\dagger_{\boldsymbol{k}+\boldsymbol{q}} \hat{h}^\dagger_{\boldsymbol{k}'-\boldsymbol{q}} \hat{h}_{\boldsymbol{k}'} \hat{h}_{\boldsymbol{k}} - 2\hat{c}^\dagger_{\boldsymbol{k}+\boldsymbol{q}} \hat{h}^\dagger_{\boldsymbol{k}'-\boldsymbol{q}} \hat{h}_{\boldsymbol{k}'} \hat{c}_{\boldsymbol{k}}) \tag{37}$$

$$v(\boldsymbol{q}) = \frac{2\pi e^2}{\varepsilon_0 q} \tag{38}$$

where ε_0 is the static dielectric constant of the IQW.

(ii) The dipole–dipole interaction between the QWs, as follows from the equations (6) and (7):

$$\hat{H}_{hyb} = \sum_{\boldsymbol{k}} V_{hyb}(\boldsymbol{k}) \hat{B}^\dagger_{\boldsymbol{k}} \sum_{\boldsymbol{q}} \hat{h}_{-\boldsymbol{q}} \hat{c}_{\boldsymbol{k}+\boldsymbol{q}} + \mathrm{HC} \tag{39}$$

$$V_{hyb}(\boldsymbol{k}) = -\frac{d_i^{F*} d_j^{vc}}{a_F\sqrt{S}} \int \mathrm{d}z\ \mathcal{D}_{ij}(\boldsymbol{k}, -z_0, z) \chi^e(z)\chi^h(z) \tag{40}$$

which corresponds to (19) with $\sqrt{[2/(\pi a_B^2)]}$ replaced by $1/\sqrt{S}$ since we use plane waves as the basis for the semiconductor states. Of course, this interaction is also of Coulomb nature,

but since we treat the OQW and the IQW as completely different systems and neglect all effects of electronic exchange between them, these pieces of the Hamiltonian are separate.

(iii) The interaction with the driving electric field (34):

$$\hat{H}_{dr} = -(\boldsymbol{\mathcal{E}}_0 \cdot \boldsymbol{M}^F)\mathrm{e}^{-\mathrm{i}\omega t}\hat{B}^{\dagger}_{\boldsymbol{Q}_\parallel} - (\boldsymbol{\mathcal{E}}_0 \cdot \boldsymbol{M}^{eh})\mathrm{e}^{-\mathrm{i}\omega t}\sum_{\boldsymbol{q}} \hat{c}^{\dagger}_{\boldsymbol{Q}_\parallel+\boldsymbol{q}}\hat{h}^{\dagger}_{-\boldsymbol{q}} + \mathrm{HC} \tag{41}$$

$$\boldsymbol{M}^{eh} = \boldsymbol{d}^{vc*}\int \chi^{e*}(z)\chi^{h*}(z)\,\mathrm{d}z \qquad \boldsymbol{M}^F = \frac{\sqrt{S}}{a_F}\boldsymbol{d}^{F*} \tag{42}$$

where we again neglect the z-dependence of the field and the wavevector dependence of $\boldsymbol{M}^{eh}$.

Given the Hamiltonian, we can write down the equations of motion for the Heisenberg operators. The polarization is obtained by averaging the expressions (35), (36) over the equilibrium density matrix. The result is expressed in terms of the polarization functions

$$\left\langle \hat{h}_{-\boldsymbol{q}}(t)\hat{c}_{\boldsymbol{k}+\boldsymbol{q}}(t)\right\rangle = \mathcal{P}^W_{\boldsymbol{k}}(\boldsymbol{q}) \qquad \left\langle \hat{B}_{\boldsymbol{k}}(t)\right\rangle = \mathcal{P}^F_{\boldsymbol{k}}. \tag{43}$$

Average values of the four-operator terms are factorized in the Hartree–Fock approximation and are expressed in terms of the polarization functions and the populations defined by

$$\left\langle \hat{c}^{\dagger}_{\boldsymbol{q}}(t)\hat{c}_{\boldsymbol{q}'}(t)\right\rangle = \delta_{\boldsymbol{q}\boldsymbol{q}'}n^e_{\boldsymbol{q}} \qquad \left\langle \hat{h}^{\dagger}_{\boldsymbol{q}}(t)\hat{h}_{\boldsymbol{q}'}(t)\right\rangle = \delta_{\boldsymbol{q}\boldsymbol{q}'}n^h_{\boldsymbol{q}}. \tag{44}$$

Here the averages with different wavevectors correspond to the intraband polarization, which is far off resonance and may be neglected. Since the electric field excites only states with the given total in-plane wavevector $\boldsymbol{Q}_\parallel$, from now on we set $\boldsymbol{k} = \boldsymbol{Q}_\parallel$. As a result, we obtain generalized Bloch equations for the polarization functions:

$$\mathrm{i}\hbar\frac{\mathrm{d}\mathcal{P}^F_{\boldsymbol{k}}}{\mathrm{d}t} = E_F(\boldsymbol{k})\mathcal{P}^F_{\boldsymbol{k}} + V_{hyb}(\boldsymbol{k})\sum_{\boldsymbol{q}}\mathcal{P}^W_{\boldsymbol{k}}(\boldsymbol{q}) - (\boldsymbol{\mathcal{E}}_0\boldsymbol{M}^F)\mathrm{e}^{-\mathrm{i}\omega t} \tag{45}$$

$$\mathrm{i}\hbar\frac{\mathrm{d}\mathcal{P}^W_{\boldsymbol{k}}(\boldsymbol{q})}{\mathrm{d}t} = \hat{\mathcal{H}}_0\mathcal{P}^W_{\boldsymbol{k}}(\boldsymbol{q}) + \hat{\mathcal{H}}_1\mathcal{P}^W_{\boldsymbol{k}}(\boldsymbol{q}) + (1 - n^e_{\boldsymbol{k}+\boldsymbol{q}} - n^h_{-\boldsymbol{q}})\left[V^*_{hyb}(\boldsymbol{k})\mathcal{P}^F_{\boldsymbol{k}} - (\boldsymbol{\mathcal{E}}_0\boldsymbol{M}^{eh})\mathrm{e}^{-\mathrm{i}\omega t}\right] \tag{46}$$

$$\hat{\mathcal{H}}_0\mathcal{P}^W_{\boldsymbol{k}}(\boldsymbol{q}) \equiv [\varepsilon_e(\boldsymbol{k}+\boldsymbol{q}) + \varepsilon_h(-\boldsymbol{q})]\,\mathcal{P}^W_{\boldsymbol{k}}(\boldsymbol{q}) - \sum_{\boldsymbol{q}'}\frac{v(\boldsymbol{q}-\boldsymbol{q}')}{S}\mathcal{P}^W_{\boldsymbol{k}}(\boldsymbol{q}')$$

$$\hat{\mathcal{H}}_1\mathcal{P}^W_{\boldsymbol{k}}(\boldsymbol{q}) \equiv -\left[\sum_{\boldsymbol{q}'}\frac{v(\boldsymbol{q}-\boldsymbol{q}')}{S}(n^e_{\boldsymbol{k}+\boldsymbol{q}'} + n^h_{-\boldsymbol{q}'})\right]\mathcal{P}^W_{\boldsymbol{k}}(\boldsymbol{q}) + (n^e_{\boldsymbol{k}+\boldsymbol{q}} + n^h_{-\boldsymbol{q}})\sum_{\boldsymbol{q}'}\frac{v(\boldsymbol{q}-\boldsymbol{q}')}{S}\mathcal{P}^W_{\boldsymbol{k}}(\boldsymbol{q}').$$

Here the 'Hamiltonian' $\hat{\mathcal{H}}_0$ describes the evolution of the polarization in an isolated IQW in the absence of electron–hole populations and corresponds to the Wannier equation [20]. The resonant Wannier exciton wavefunction in the momentum space $\Phi_{\boldsymbol{k}}(\boldsymbol{q})$ is its eigenfunction with the eigenvalue $E_W(\boldsymbol{k})$. The 'Hamiltonian' $\hat{\mathcal{H}}_1$ describes the nonlinear many-particle corrections. It is proportional to the populations n^e, n^h and we treat it perturbatively, keeping only the first-order corrections to the eigenfunction $\delta\Phi_{\boldsymbol{k}}(\boldsymbol{q})$ and to the eigenvalue $\delta E_W(\boldsymbol{k})$. Since populations are proportional to the intensity of the applied field $|\mathcal{E}_0|^2$, our calculation describes a third-order nonlinearity.

We seek the solutions depending on time as $\mathrm{e}^{-\mathrm{i}\omega t}$. The solution for $\mathcal{P}^W_{\boldsymbol{k}}(\boldsymbol{q})$ may be expressed in terms of the orthonormal basis of eigenfunctions of $\hat{\mathcal{H}}_0 + \hat{\mathcal{H}}_1$. Picking up just the resonant term, we may write

$$\mathcal{P}^W_{\boldsymbol{k}}(\boldsymbol{q}) = u^W_{\boldsymbol{k}}\big(\Phi_{\boldsymbol{k}}(\boldsymbol{q}) + \delta\Phi_{\boldsymbol{k}}(\boldsymbol{q})\big)\mathrm{e}^{-\mathrm{i}\omega t} \tag{47}$$

$$u^W_{\boldsymbol{k}}\mathrm{e}^{-\mathrm{i}\omega t} = \sum_{\boldsymbol{q}}\big(\Phi^*_{\boldsymbol{k}}(\boldsymbol{q}) + \delta\Phi^*_{\boldsymbol{k}}(\boldsymbol{q})\big)\mathcal{P}^W_{\boldsymbol{k}}(\boldsymbol{q}) \tag{48}$$

$$\mathcal{P}^F_{\boldsymbol{k}} = u^F_{\boldsymbol{k}}\mathrm{e}^{-\mathrm{i}\omega t}. \tag{49}$$

Then equations (45), (46) are reduced to

$$\begin{aligned}\big(\hbar\omega - E_F(\boldsymbol{k})\big)u^F_{\boldsymbol{k}} &= V_{FW}(\boldsymbol{k})u^W_{\boldsymbol{k}} - J_F\\ \big(\hbar\omega - E_W(\boldsymbol{k}) - \delta E_W(\boldsymbol{k})\big)u^W_{\boldsymbol{k}} &= \beta_{\boldsymbol{k}}V^*_{FW}(\boldsymbol{k})u^F_{\boldsymbol{k}} - \beta_{\boldsymbol{k}}J_W\end{aligned} \tag{50}$$

where we have introduced the coupling matrix element

$$V_{FW}(\boldsymbol{k}) + \delta V_{FW}(\boldsymbol{k}) = V_{hyb}(\boldsymbol{k})\sum_{\boldsymbol{q}}\big(\Phi_{\boldsymbol{k}}(\boldsymbol{q}) + \delta\Phi_{\boldsymbol{k}}(\boldsymbol{q})\big) \tag{51}$$

and the effective driving forces

$$J_F = \boldsymbol{\mathcal{E}}_0 \cdot \boldsymbol{M}^F \qquad J_W + \delta J_W = \boldsymbol{\mathcal{E}}_0 \cdot \boldsymbol{M}^{eh}\sum_{\boldsymbol{q}}\big(\Phi^*_{\boldsymbol{k}}(\boldsymbol{q}) + \delta\Phi^*_{\boldsymbol{k}}(\boldsymbol{q})\big) \tag{52}$$

and also the Pauli blocking factor given by

$$\beta_{\boldsymbol{k}} = \left(\sum_{\boldsymbol{q}}(1 - n^e_{\boldsymbol{k}+\boldsymbol{q}} - n^h_{-\boldsymbol{q}})\Phi^*_{\boldsymbol{k}}(\boldsymbol{q})\right)\Big/\left(\sum_{\boldsymbol{q}}\Phi^*_{\boldsymbol{k}}(\boldsymbol{q})\right). \tag{53}$$

In the low-density limit and with $\mathcal{E}_0 = 0$, these equations correspond to the eigenvalue equation (2) with the coupling matrix elements given by (19), since for 1s excitons

$$\Phi_{\boldsymbol{k}}(\boldsymbol{q}) = \sqrt{\frac{8\pi a_B^2}{S}}\frac{1}{(q^2a_B^2 + 1)^{3/2}} \qquad \sum_{\boldsymbol{q}}\Phi_{\boldsymbol{k}}(\boldsymbol{q}) = \sqrt{2S/(\pi a_B^2)}. \tag{54}$$

Solving the system (50), we obtain for the polarization of the structure under consideration (per unit area)

$$\begin{aligned}P^s_i(\boldsymbol{r}_\parallel) \equiv \int\left\langle\hat{P}^F_i(\boldsymbol{r}) + \hat{P}^W_i(\boldsymbol{r})\right\rangle\,\mathrm{d}z &\simeq \frac{u^F_{\boldsymbol{k}}M^{F*}_i}{S}\mathrm{e}^{-\mathrm{i}\omega t + \mathrm{i}\boldsymbol{k}\cdot\boldsymbol{r}_\parallel} + \mathrm{CC}\\ &= \chi_{ij}(\omega, \boldsymbol{k})\mathcal{E}_{0j}\mathrm{e}^{-\mathrm{i}\omega t + \mathrm{i}\boldsymbol{k}\cdot\boldsymbol{r}_\parallel} + \mathrm{CC}\end{aligned} \tag{55}$$

where we have retained only the term proportional to $|\boldsymbol{M}^F|^2$ since $|J_W| \ll |J_F|$. Finally, we obtain for the susceptibility (not forgetting the factor of 2 originating from spin degeneracy as mentioned at the beginning of this subsection)

$$\chi_{ij}(\omega, \boldsymbol{k}) = 2\frac{d^{F*}_i d^F_j}{a_F^2}\frac{E_W(\boldsymbol{k}) + \delta E_W(\boldsymbol{k}) - \hbar\omega}{(E_W(\boldsymbol{k}) + \delta E_W(\boldsymbol{k}) - \hbar\omega)(E_F(\boldsymbol{k}) - \hbar\omega) - \beta_{\boldsymbol{k}}|V_{FW}(\boldsymbol{k}) + \delta V_{FW}(\boldsymbol{k})|^2}. \tag{56}$$

In equation (56) the nonlinearities appear through the blue-shift δE_W, the blocking factor β and the modification of the hybridization δV_{FW} due to the correction $\delta\Phi$; all of these effects are typical of Wannier excitons [13], but here they belong to the hybrid excitons which also have a large oscillator strength characteristic of Frenkel excitons. When

only excitons are present (i.e., under resonant excitation at low temperature), the nonlinear corrections can be calculated to first order in the ns with

$$n^e_{k+q} = n^h_{-q} \simeq \frac{n_T S}{4}|\Phi_k(q)|^2 \tag{57}$$

where n_T is the total density of electron–hole pairs and the factor $1/4$ takes into account electron (and hole) spin degeneracy of two and an equal population of resonant FE and WE. In terms of the previous subsection, this corresponds to the situation when $k \simeq k_0$; thus $E_F(k) \simeq E_W(k)$, $|A_\alpha|^2 \simeq |B_\alpha|^2 \simeq 1/2$ and $|u^F_k|^2 \simeq |u^W_k|^2 \simeq (n_T S)/4$. The blue-shift δE_W is given by the expectation value of $\mathcal{H}_1$ on $\Phi_k(q)$ and reduces to

$$\delta E_W \simeq 0.48 E_b \pi a_B^2 n_T \tag{58}$$

where E_b is the binding energy of a 2D Wannier exciton. The blocking factor is calculated from equation (53) and turns out to be

$$\beta_k \simeq 1 - 0.57\pi a_B^2 n_T. \tag{59}$$

The effect of δV_{FW} can be estimated [13] by writing $\delta\Phi_k(q)$ as a sum over all continuous and discrete excitonic states which are then approximated by plane waves in the expression for $|V_{FW} + \delta V_{FW}|^2$, giving

$$|V_{FW} + \delta V_{FW}|^2 \simeq (1 - 0.48\pi a_B^2 n_T)|V_{FW}|^2. \tag{60}$$

Close to resonance (denoting the detuning $\hbar\omega - E_W(k)$ by ΔE), equation (56) can be approximated by

$$\begin{aligned}\chi_{ij}(\omega, k) &= -2\frac{d_i^{F*} d_j^F}{a_F^2}\frac{\Delta E}{\Delta E^2 - |V_F W|^2} \\ &\quad \times \left[1 - \pi a_B^2 n_T\left(\frac{1.05|V_{FW}|^2 - 0.48E_b\Delta E}{\Delta E^2 - |V_{FW}|^2} + \frac{0.48E_b}{\Delta E}\right)\right] \\ &= \chi^{(1)}_{ij}(\omega, k)\left(1 - \frac{n_T}{n_S}\right)\end{aligned} \tag{61}$$

where $\chi^{(1)}_{ij}(\omega, k)$ is the susceptibility of the hybrid structure at $n_T = 0$ (the linear susceptibility) and n_S is the saturation density. The characteristic feature of the expression (61) is the presence of the factor $(d^F/a_F)^2$ in $\chi^{(1)}$ instead of $(d^{vc}/a_B)^2$ in the analogous expression for an isolated IQW. This leads to the enhancement of the absorption, determined by Im $\chi^{(1)}$. Thus, while the saturation density is comparable to that of Wannier excitons ($n_S \sim 1/a_B^2$), the density of photogenerated electron–hole pairs, for a given light intensity, can be two orders of magnitude larger (by a factor $\sim(a_B/a_F)^2$); for the same reason, the linear susceptibility $\chi^{(1)}$ can also be two orders of magnitude larger. Therefore, the present theory substantiates the intuitive expectation of very pronounced nonlinear optical properties of the hybrid excitons.

While the range of validity of equation (61) (with respect to variations of ΔE and n_T) is rather limited, the expression for χ given by equation (56) holds true as long as the basic approximations of the present approach are tenable. These are, in addition to the first-order perturbation theory with respect to the excitation density n_T, the usual Hartree–Fock decoupling in the equations of motion adopted in equations (45), (46), the subsistence of well defined individual excitons (valid only for $n_T \lesssim n_S$) and the neglect of screening due to the reduced screening efficiency of a two-dimensional exciton gas [13, 20]. Numerical examples of the predictions of equation (56) have been obtained using the values of semiconductor parameters representative of III–V semiconductor (e.g., GaAs/AlGaAs)

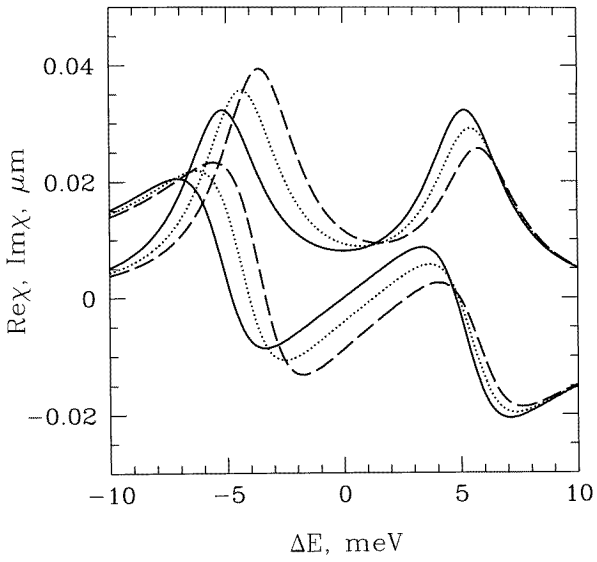

Figure 6. Real and imaginary parts of the 2D susceptibility χ near the hybrid exciton resonances in the linear regime (solid lines), for medium excitation density ($n_T = 10^{11}$ cm^{-2}; dotted lines) and for high excitation density ($n_T = 2 \times 10^{11}$ cm^{-2}; long-dashed lines). The other parameters are $d^{vc} = 20$ D, $a_B = 60$ Å $E_b = 20$ meV, $\varepsilon_\infty = 11$; the rest are the same as in the previous subsection. The linewidths $\hbar\gamma_W = \hbar\gamma_F = 2$ meV.

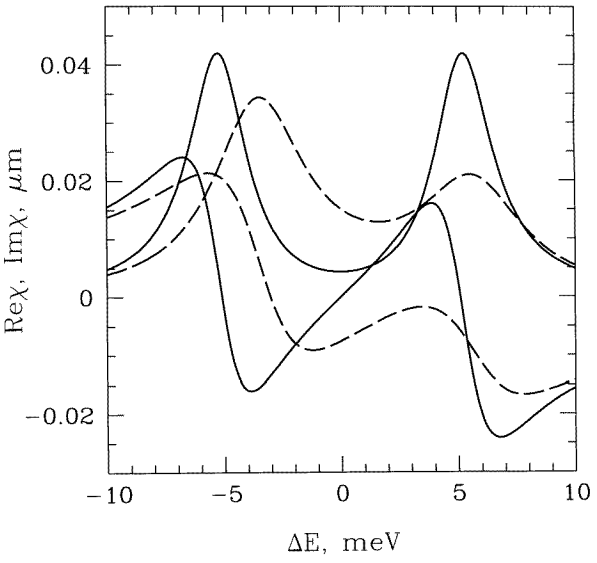

Figure 7. Real and imaginary parts of χ in the linear regime (solid lines) and for high excitation density ($n = 2 \times 10^{11}$ cm^{-2}; long-dashed lines); in the first case $\hbar\gamma_W = 1$ meV, while in the second case $\hbar\gamma_W = 3$ meV.

quantum wells, since the necessary information on homogeneous linewidths of excitons in II–VI QWs is not currently available to the authors. Namely, we set $\varepsilon_\infty = 11$, $d^{vc} = 20$ D,

the Bohr radius $a_B = 60$ Å and the binding energy is taken to be $E_b \simeq 20$ meV; the rest are the same as in the previous subsection. This gives $|V_{FW}| \simeq 4$ meV at $k = 10^7$ cm^{-1}. Assuming a phenomenological linewidth $\hbar\gamma_W = \hbar\gamma_F = 2$ meV for both excitons, figure 6 shows the split resonance of the hybrid excitons at different excitation densities (linear regime, $n_T = 10^{11}$ cm^{-2} and $n_T = 2 \times 10^{11}$ cm^{-2}); it is noticeable, in particular, that for vanishing excitation density the mixing is complete and the oscillator strength is equally shared by the two peaks, whereas for high excitation density, due to the small blue-shift of the WE, the stronger line corresponds to the lowest (more Frenkel-like) hybrid exciton. Figure 7 shows the effect of a density-dependent broadening of the Wannier exciton: $\hbar\gamma_W = 1$ meV at low excitation densities and $\hbar\gamma_W = 3$ meV at high excitation density [21] ($\hbar\gamma_F$ being fixed at 2 meV). From numerical estimates such as those shown in figures 6 and 7, we obtain for the relative nonlinear change in the absorption coefficient close to resonance $|\Delta\alpha|/\alpha \sim 10^{-11}$ cm^2 n_T, which is analogous to the case of a semiconductor multiple quantum well. However, for a given pump intensity, the 2D density of photogenerated excitons n_T in our case of hybrid excitons is about two orders of magnitude larger because the oscillator strength of hybrid excitons is comparable to that of Frenkel excitons rather than that of Wannier excitons.

A similar theoretical approach can be used to calculate the dynamical Stark effect for hybrid excitons, which shows qualitative and quantitative differences with respect to the case of the usual inorganic semiconductor QWs [22].

2.2.2. Second-order susceptibility $\chi^{(2)}$. As was already mentioned, the calculations, performed here, correspond to the third-order nonlinearity. But the hybrid system considered here has also a nonzero second-order susceptibility $\chi^{(2)}$. For such structure, $\chi^{(2)} \neq 0$ even if the original OQW and IQW are centro-symmetric and the second-order processes are forbidden by parity conservation. Such a phenomenon can take place because the resonant dipole–dipole coupling breaks the symmetry along the growth direction. Of course, any interaction between the OQW and the IQW can be responsible for symmetry breaking. However, the resonant dipole–dipole coupling considered here is probably the strongest among the possibilities. In a geometrical sense, this system is analogous to an asymmetric semiconductor QW. The calculation of $\chi^{(2)}$ for such a system can be found in reference [23] and the calculation of $\chi^{(2)}$ for the hybrid system may be performed following the lines of the latter work.

A detailed calculation of the second-order nonlinear susceptibility of the hybrid structure will be published elsewhere. Here we restrict ourselves to some qualitative remarks. The general microscopic expression for the nth-order susceptibility contains $n+1$ dipole moment matrix elements, involving n intermediate states. For the linear susceptibility there is only one intermediate state, and if the latter is a hybrid one, the corresponding dipole matrix elements are determined mainly by the Frenkel component of the hybrid state. Thus, the linear susceptibility of the hybrid structure contains the factor $(d^F/a_F)^2$, as is seen from equation (61). For the second-order nonlinear susceptibility $\chi^{(2)}$ one must have two intermediate states or three virtual transitions. One of them may be a hybrid one, and as long as the materials under consideration have no static dipole moments, the other intermediate state has to be an excited state of the IQW, which is not resonant with the Frenkel exciton. Hence, the result will be proportional to d^F/a_F; the other two virtual transitions will give the factor, coinciding with that for an isolated IQW. One may apply analogous arguments to the case of the third-order nonlinearity: of three intermediate states needed, one may be the hybrid one, the second may be the ground state and the third one may be again the

hybrid state (such a scheme corresponds to the Kerr nonlinearity). Thus, one should obtain a factor $(d^F/a_F)^4$. Indeed, in equation (61) we have $(d^F/a_F)^2$ in $\chi^{(1)}$ and another factor, $(d^F/a_F)^2$, comes from n_T when the latter is expressed in terms of the incident electric field.

There exists another mechanism for second-harmonic generation. It does not require parity breaking, since the optical quadratic nonlinearity appears due to the contribution of spatial derivatives of the electric field to the nonlinear response [24, 25]. It works also in the case of an isolated symmetric QW and corresponds to a higher multipole contribution rather than the dipole one, which is usually considered. The hybrid system will again have an advantage here because of the increase in the oscillator strength due to the Frenkel exciton component.

2.3. Hybrid excitons in other heterostructures

Hybrid states of Frenkel and Wannier–Mott excitons were also considered for other geometries, such as quasi-1D parallel organic and inorganic quantum wires [26] as well as in a spherical system (quantum dot) [27]. We do not analyse here the experimental possibilities of constructing such systems and mention only some essential points which are different from those in the plane geometry studied above.

An important feature of the hybrid states in quasi-1D systems is the fact that the matrix element of the resonant dipole–dipole coupling between the quantum wires is different from zero even at zero wavevector (which is not the case for 2D systems). This makes it possible to excite these states directly without involving any special methods (such as using coupled gratings or attenuated total reflection). Evidently, an analogous situation arises in the case of quantum dots, where the states cannot be described by the wavevector at all.

In reference [27] the third-order nonlinear susceptibility $\chi^{(3)}$ for a semiconductor quantum dot covered with organic material was found. In this work it was assumed that the inhomogeneous broadening in the organic material is absent and it is possible to consider Frenkel excitonic states. Similarly to the 2D case (section 2.2), a strong enhancement of $\chi^{(3)}$ near the hybrid exciton resonance was predicted.

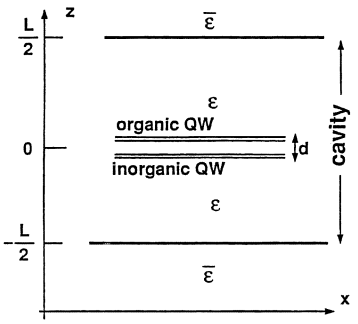

Figure 8. A schematic diagram of microcavity-embedded organic and inorganic quantum wells. The mirrors are simply described by a very high dielectric constant $\bar{\varepsilon} \gg \varepsilon$.

2.4. Microcavity configurations

The structure described in section 2.1 presents the technologically challenging problem of growing high-quality organic–inorganic heterojunctions only a few nanometres apart. A

more promising way of realizing a hybrid exciton system is to couple Frenkel and Wannier excitons through a microcavity (MC) electromagnetic field [28]. Strong exciton–radiation interactions are observed in microcavities [29] and we can expect hybridization to arise not due to the Coulombic short-range interaction, but due to the strong long-range interaction stemming from virtual-cavity-photon exchange. For cavity-embedded QWs, the fabrication problems would be much alleviated as their separation can be of the order of an optical wavelength. For the sake of simplicity, however, in the following discussion we assume that both QWs lie at the centre ($z \simeq 0$) of a single MC at a distance $d \ll \lambda$ from each other (see figure 8). This situation is qualitatively equivalent to that of two coupled microcavities for which the growth conditions could be separately optimized for the organic and inorganic well [28].

Microcavity-embedded organic QWs in the weak-coupling regime have already been realized [30] and effects such as spectral narrowing and increased directionality of light emission demonstrated. To achieve the strong-coupling regime, as observed for inorganic QWs [29], with organic materials, we need molecular compounds combining a large oscillator strength of the lowest-energy electronic transition with an absorption linewidth smaller than the cavity mode splitting. Good candidates for such structures are thin-film crystals of aromatic molecules like anthracene, tetracene, terrylene and many others. For example, five monolayers of terrylene ($d \simeq 50$ Å) exhibit an oscillator strength per unit area as large as 10^{15} cm^{-2}, more than a hundred times that of a GaAs QW exciton.

In order to illustrate the results obtained for such a system [28], we use for the material parameters data from available experiments or realistic estimates. We assume that $E_F(k) = E_C(k = 0)$ and $E_W(k = 0) = E_C(k = 0)(1 + \eta)$, i.e. a Frenkel exciton resonant with the cavity mode E_C (we neglect the dispersion of the FE) and a Wannier exciton with a fractional detuning of η at $k = 0$. Using the reduced variable $\bar{k} = k/k_{cav}$ with $k_{cav} = \pi/L$, we have for this case

$$E_C(k)/E_C(0) = \sqrt{1 + \bar{k}^2} \qquad E_W(k)/E_W(0) = 1 + \eta + a\bar{k}^2$$

with $a = \hbar^2 k_{cav}^2/2ME_C(0)$. For resonance at $E_C(0) = 1.5$ eV and $\varepsilon \simeq 10$, we have $k_{cav} = 2.4 \times 10^5$ cm^{-1} and, using an exciton mass $M = 0.3m_0$ (m_0 is the free-electron mass), $a = 10^{-5}$. The inorganic QW Rabi splitting Δ_1 is taken to be 3 meV; then, assuming a ratio of the organic to the inorganic QW oscillator strength $F/f \simeq 60$, we have for the organic QW Rabi splitting $\Delta_2 \simeq 23$ meV. The ratio $\Delta_2/\Delta_1 \simeq 8$ is by no means unusually large and, as a matter of fact, even larger oscillator strengths can easily be attained with many organic materials. For example, from the standard LT splittings of 0.08 meV in GaAs ($\varepsilon \simeq 12$) and $\simeq$50 meV for the lowest singlet exciton in tetracene ($\varepsilon \simeq 9$) [31], their oscillator strength ratio is about 500. The large splittings $\Delta_2 \approx 100$ meV expected from such estimates gave reasonable hope for reaching the strong-coupling regime even at room temperature since the absorption linewidth can be as low as a few tens of meV in selected organic systems.

In fact, very recently and for the first time, the strong-coupling regime in a MC with an organic active layer has been observed [32] employing several organic compounds. For example, using the organic semiconductor tetra-(2, 6-*tert*-butyl)phenol-porphyrin zinc (4TBPPZn), a splitting $\Delta_2 \simeq 100$ meV has been found. In this case, the thickness L_2 of the active layer was about 1000 Å and, as $\Delta_2 \propto \sqrt{L_2}$, such an experimental value [32] corresponds very well to the estimate of $\Delta_2 \simeq 25$ meV [28] made for $L_2 \simeq 50$ Å. In these experiments [32], different dyes have been blended in a polymer matrix to realize active thin films. In order to suppress the inhomogeneous broadening and also to further enhance the mode splitting, it is very important to employ crystalline organic semiconductors. We are

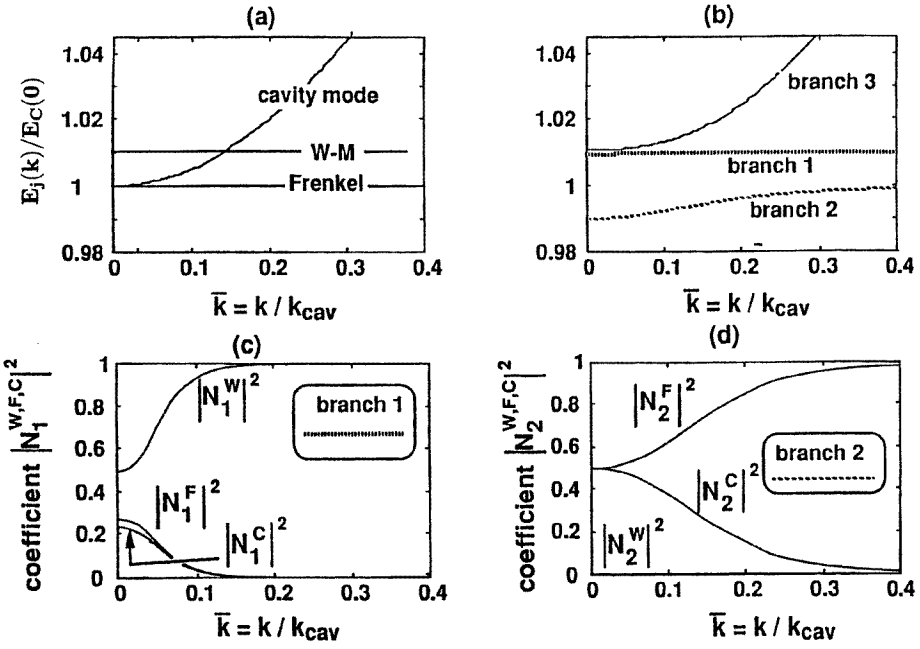

Figure 9. (a) Bare dispersion curves of a cavity photon, with the WE and FE normalized to the cavity mode at $k = 0$. The FE exciton is resonant with the cavity mode and the WE has a positive detuning. (b) Cavity polariton dispersion curves: for large wavevectors; branches 1, 2 and 3 turn into WE, FE and cavity photons, respectively. (c) Weighting coefficients of branch 1. (d) Weighting coefficients of branch 2.

confident that in exactly this way it will be possible to observe the Frenkel–Wannier–Mott exciton hybridization in an organic MC.

We assume such a situation in our demonstration calculations and neglect dissipation for both bare excitonic states. The dispersion of cavity polaritons $E_j(k)$ and of the weighting coefficients $N_j^{F,W,C}(k)$ (analogous to A and B of equation (1)) are shown in figure 9. From figure 9(c) it is seen that the branch 1 (which at large wavevectors turns into a pure WE) contains a major part of a FE state ($|N_1^F|^2$) for $\bar{k} < 0.1$. As seen from figure 9(d), the branch 2 (which at large wavevectors turns into a pure FE) for $\bar{k} < 0.25$ also retains a major part of a FE state ($|N_2^F|^2$) while exhibiting a large cavity photon component. The FE component is crucial in assisting the inelastic relaxation that will be considered, whereas the cavity photon component obviously has a large radiative width. For $\bar{k} \ll 1$ even for high mirror reflectivities ($1 - R = 10^{-3}$), the cavity mode radiative lifetime is of order $\tau \simeq 1$ ps. The better mixing of branch 2 with the cavity photon means faster radiative decay in a larger phase space. Such a short lifetime is only effective in a very narrow region of phase space ($k < 0.05k_{cav}$) in the case of typical inorganic QW splittings; such a region can only be reached in about 100 ps due to slowed-down relaxation [33] in the flat part of the dispersion curve, poorly coupled to the cavity mode. In our case, to populate the states of branch 2 with a large radiative width (i.e., those with $k < 0.2k_{cav}$), we can assume that the parameters of the MC with two QWs are such that for $k, k' < 0.2k_{cav}$ an inelastic resonance condition is realized, i.e. that the energy difference $E_1(k) - E_2(k')$ is close to the energy of some intramolecular optical phonon strongly coupled to excitons. For this case,

the relaxation rate can be of order 10 ps or less [28], i.e. at least one order of magnitude faster than for MC with an inorganic QW.

Summarizing, we have considered the new possibilities which may appear for microcavities containing resonating organic and inorganic QWs. Although our estimates are preliminary, we can expect in such structures a drastic reduction of the relaxation time of excitons to give states having a large radiative width and a short fluorescence decay time. We can also expect that the combination of electrical pumping of excitons in inorganic QWs with the fast relaxation and fluorescence of excitons in organic QWs will open up a new scenario of excitonic processes in microcavities, of interest for both basic science and device applications.

3. Förster resonant energy transfer from a semiconductor QW to organics

In this section we study the situation in which the width of the excitonic resonance in the organic material is larger than possible hybrid excitons' frequency shifts or splitting (the weak-coupling regime). Then, instead of a coherent hybridization of excitonic states the dipole–dipole (Förster) energy transfer from the IQW to the organic material has to be considered. This case was analysed in detail in references [34, 35].

The configuration that we consider consists of a semiconductor quantum well sandwiched between two semiconductor barriers, the whole semiconductor structure embedded in bulk-like organic material (for the sake of simplicity, we choose a symmetric configuration and consider the organic material to be isotropic). The background dielectric constant of the semiconductor material is taken to be real, whereas the total dielectric constant of the organic material has both a real and an imaginary part in the frequency region of interest. In fact, we are interested in an organic material having a broad absorption band in the optical range overlapping with the two-dimensional Wannier–Mott exciton sharp resonance. We consider both cases of a free Wannier–Mott exciton as well as of a localized one due to the alloy disorder and QW width fluctuations.

The Förster-like rate of energy transfer due to the dipole–dipole interaction can be calculated simply from the Joule losses [36] in the organic material. The details are presented in reference [35]; here we merely summarize the general scheme. We neglect retardation, as the typical exciton centre-of-mass in-plane wavevector is much larger than the wavevector of the corresponding resonant light. We also consider only the linear regime in which excitons can be described in the bosonic approximation. Then the transfer rate may be calculated as follows.

Let the QW exciton with the energy $\hbar\omega$ be described by the envelope function $\psi(\boldsymbol{r}_e, \boldsymbol{r}_h)$, where $\boldsymbol{r}_e$, $\boldsymbol{r}_h$ are the positions of the electron and the hole, and the normalization be

$$\int \mathrm{d}^3\boldsymbol{r}_e \, \mathrm{d}^3\boldsymbol{r}_h \, |\psi(\boldsymbol{r}_e, \boldsymbol{r}_h)|^2 = 1. \tag{62}$$

Then suppose that inside the QW we have the classical macroscopic quasi-stationary polarization, oscillating with the frequency ω:

$$\boldsymbol{P}(\boldsymbol{r}, t) = \boldsymbol{d}^{vc}\psi(\boldsymbol{r}, \boldsymbol{r})\mathrm{e}^{-\mathrm{i}\omega t} + \mathrm{CC} \tag{63}$$

where $\boldsymbol{d}^{vc}$ is the matrix element (16). Then, we solve the electrostatical problem (i.e., neglecting retardation) and find the corresponding electric field:

$$\boldsymbol{\mathcal{E}}(\boldsymbol{R}, t) = \boldsymbol{\mathcal{E}}(\boldsymbol{R})\mathrm{e}^{-\mathrm{i}\omega t} + \mathrm{CC}. \tag{64}$$

The correct quantum mechanical energy transfer rate is given by the macroscopic formula

$$\frac{1}{\tau} = \frac{1}{2\pi\hbar}\int \mathrm{d}^3\boldsymbol{r}\ \mathrm{Im}\,\varepsilon_{ij}(\boldsymbol{r},\omega)\,\mathcal{E}_i(\boldsymbol{r})\mathcal{E}_j^*(\boldsymbol{r}) \tag{65}$$

where $\varepsilon_{ij}(\boldsymbol{r},\omega)$ is the complex dielectric function of the acceptor organic medium. Both the microscopic dipole approximation and the macroscopic description of the organic medium are valid as long as the electric field obtained is slowly varying in space on the molecular scale. This condition is fulfilled in all of the cases considered below, since the typical wavevectors of excitons as well as e–h pairs in the QW are small compared to the inverse lattice constant (and the localization length is larger than the lattice constant).

3.1. Free excitons

First, we specify the geometry of the problem, which is the same for all subsequent sections. We consider a symmetric structure, consisting of a semiconductor QW of thickness L_w between two barriers each of thickness L_b, the whole semiconductor structure being surrounded by thick slabs of an organic material (in fact, we assume each slab to be semi-infinite). We assume that in the frequency region considered here the semiconductor background dielectric constant ε_b is real and the same for the well and the barrier, while that of the organic material $\tilde{\varepsilon}$ is complex. For simplicity we assume the organic material to be isotropic (generalization to the anisotropic case is straightforward). So, the dielectric constant to be used in equation (65), as well as in the Poisson equation below, is

$$\varepsilon_{ij}(\boldsymbol{r}) = \begin{cases} \varepsilon_b\delta_{ij} & |z| < L_w/2 + L_b \\ \tilde{\varepsilon}\delta_{ij} & |z| > L_w/2 + L_b \end{cases} \tag{66}$$

where the z-axis is chosen to be along the growth direction, $z = 0$ corresponding to the centre of the QW.

We adopt a simplified microscopic quantum mechanical model of a quantum well Wannier–Mott exciton, in which the polarization can be taken to vanish for $|z| > L_w/2$ and that inside the well to be given by

$$\boldsymbol{P}(\boldsymbol{r}) = \boldsymbol{d}^{vc}\sqrt{\frac{2}{\pi a_B^2}}\frac{2}{L_w}\cos^2\left(\frac{\pi z}{L_w}\right)\frac{\mathrm{e}^{\mathrm{i}\boldsymbol{k}\cdot\boldsymbol{r}_\parallel}}{\sqrt{S}} \tag{67}$$

where S is the in-plane normalization area, $\boldsymbol{k}$ is the in-plane wavevector of the centre-of-mass motion, $\boldsymbol{r}_\parallel \equiv (x, y)$ is the in-plane component of $\boldsymbol{r}$ and a_B is the 2D 1s-exciton Bohr radius [5]. It is not difficult to recognize the meaning of the factors constituting (67), comparing it to (63). Namely, $\sqrt{[2/(\pi a_B^2)]}$ is the 1s wavefunction of the relative motion of the electron and hole, taken at $r_\parallel = 0$; next comes the product of the lowest-subband envelope functions for the electron and hole in the approximation of the infinitely deep well and finally the wavefunction of the centre-of-mass motion with wavevector $\boldsymbol{k}$, normalized to the area S. All of them are normalized according to (62). We choose as $\boldsymbol{x}$ the direction of the in-plane component of the exciton dipole moment $\boldsymbol{d}^{vc}$, preferring to consider the polarization with respect not to the wavevector, but to some fixed frame. This little complication is justified since following the free exciton we intend to study the case of the localized exciton, i.e., a system with broken 2D translational symmetry. Evidently, we need to consider two cases: $\boldsymbol{d}^{vc}$ being parallel and perpendicular to the QW plane. We will refer to them as X- and Z-polarizations respectively.

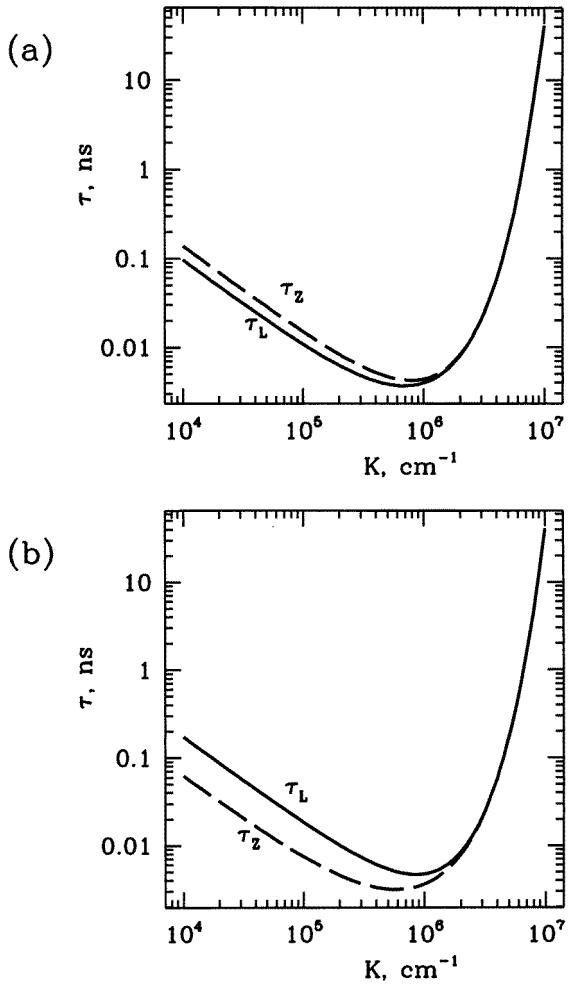

Figure 10. (a) The free-L-exciton (solid line) and free-Z-exciton (dashed line) lifetimes τ (ns) versus the in-plane wavevector K (cm^{-1}). $d^{vc}/ea_B = 0.1$, $L_w = 60$ Å, $L_b = 40$ Å, $\varepsilon_b = 6$, $\tilde{\varepsilon} = 4 + 3\mathrm{i}$. (b) The same, but for $\varepsilon_b = 4$, $\tilde{\varepsilon} = 6 + 3\mathrm{i}$.

The corresponding electric field $\boldsymbol{\mathcal{E}}(\boldsymbol{r}) = -\boldsymbol{\nabla}\varphi(\boldsymbol{r})$ can be obtained from the solution of the Poisson equation (the charge density being $\rho(\boldsymbol{r}) \equiv -\boldsymbol{\nabla}\cdot\boldsymbol{P}(\boldsymbol{r})$)

$$\varepsilon(z)\nabla^2\varphi(\boldsymbol{r}) = 4\pi\boldsymbol{\nabla}\cdot\boldsymbol{P}(\boldsymbol{r}) \tag{68}$$

with the appropriate boundary conditions at $z = \pm L_w/2$ and at $z = \pm(L_w/2 + L_b)$, i.e., continuity of the tangential component of the electric field $\boldsymbol{\mathcal{E}}(\boldsymbol{r})$ and of the normal component of the electric displacement $\boldsymbol{D}(\boldsymbol{r}) = \varepsilon(z)\boldsymbol{\mathcal{E}}(\boldsymbol{r})$. Writing $\varphi(\boldsymbol{r}) = \phi(z)\mathrm{e}^{\mathrm{i}\boldsymbol{k}\cdot\boldsymbol{r}_\parallel}$, we have the equation for $\phi(z)$:

$$\left[\frac{\mathrm{d}^2}{\mathrm{d}z^2} - k^2\right]\phi(z) = \begin{cases} 4\pi\rho(z)/\varepsilon_b & |z| < L_w/2 \\ 0 & |z| > L_w/2 \end{cases} \tag{69}$$

where

$$\rho^{(X)}(z) = \mathrm{i}k_x L_w \rho_0 (1 + \cos qz) \tag{70}$$

$$\rho^{(Z)}(z) = -qL_w \rho_0 \sin qz \tag{71}$$

$$\rho_0 = \sqrt{\frac{2}{\pi a_B^2}} \frac{d^{vc}}{\sqrt{S} L_w^2} \qquad q \equiv 2\pi / L_w \tag{72}$$

with the boundary conditions that $\phi(z)$ and $\varepsilon(z)\,\mathrm{d}\phi(z)/\mathrm{d}z$ should be continuous at the four interfaces. The corresponding solution in the organic material (for $z > L_w/2 + L_b$) is given by

$$\phi(z) = \rho_0 C_{\boldsymbol{k}} \mathrm{e}^{-k(z - L_b - L_w/2)} \tag{73}$$

$$C_{\boldsymbol{k}}^{(X)} = -\frac{\mathrm{i}k_x}{k} \frac{8\pi^2 q}{k(k^2 + q^2)} \frac{\sinh(kL_w/2)}{\varepsilon_b \sinh(kL_b + kL_w/2) + \tilde{\varepsilon} \cosh(kL_b + kL_w/2)} \tag{74}$$

$$C_{\boldsymbol{k}}^{(Z)} = \frac{8\pi^2 q}{k(k^2 + q^2)} \frac{\sinh(kL_w/2)}{\varepsilon_b \cosh(kL_b + kL_w/2) + \tilde{\varepsilon} \sinh(kL_b + kL_w/2)}. \tag{75}$$

Thus, the electric field penetrating the organic material is given by

$$\boldsymbol{\mathcal{E}}(\boldsymbol{r}) = [-\mathrm{i}\boldsymbol{k} + k\boldsymbol{e}_z]\phi(z)\mathrm{e}^{\mathrm{i}\boldsymbol{k}\cdot\boldsymbol{r}_\parallel}. \tag{76}$$

Now we simply substitute this electric field into (65) and get the decay rate:

$$\frac{1}{\tau} = \frac{S}{2\pi\hbar} \operatorname{Im}\tilde{\varepsilon} \int_{L_b + L_w/2}^{+\infty} 2k^2 |\phi(z)|^2 \,\mathrm{d}z = \frac{\operatorname{Im}\tilde{\varepsilon}}{\pi^2 \hbar} \frac{|d^{vc}|^2}{a_B^2} \frac{k|C_{\boldsymbol{k}}|^2}{L_w^4} \tag{77}$$

where we have considered the absorption only at $z > L_w/2 + L_b$ (considering also the organic material in $z < -L_w/2 - L_b$, τ would be half the size).

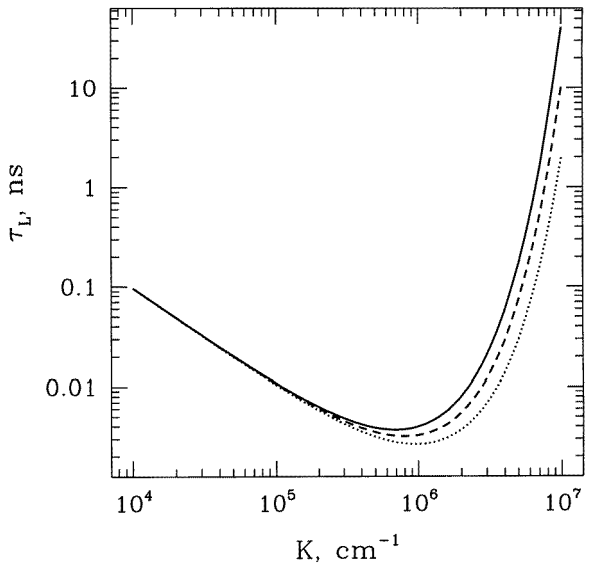

Figure 11. The free-L-exciton lifetime τ (ns) versus the in-plane wavevector K (cm^{-1}) for three well widths: $L_w = 20$ Å (dotted line), $L_w = 40$ Å (dashed line), $L_w = 60$ Å (solid line). The other parameters are $L_b = 40$ Å, $\varepsilon_b = 6$, $\tilde{\varepsilon} = 4 + 3\mathrm{i}$.

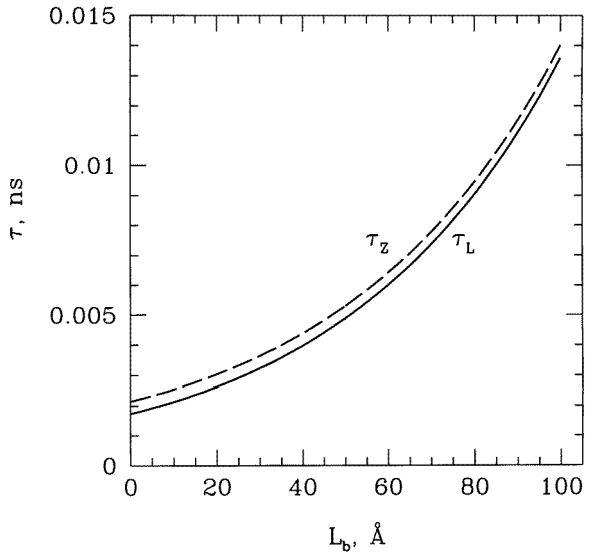

Figure 12. The free-L-exciton (solid line) and free-Z-exciton (dashed line) lifetimes τ (ns) versus the barrier width L_b (Å). $K = 10^6$ cm^{-1}, $L_w = 60$ Å, $\varepsilon_b = 6$, $\tilde{\varepsilon} = 4 + 3$i.

We evaluate τ from equation (77) for parameters representative of II–VI semiconductor QWs (analogously to section 2.1: $\varepsilon_b \approx 6$, $d^{vc} \approx 0.1ea_B$; for the organic material we take $\tilde{\varepsilon} = 4 + 3$i). We consider two cases: $\boldsymbol{d}^{vc}$ lying in the QW plane, $\boldsymbol{k} \parallel \boldsymbol{d}^{vc}$ (L-excitons) and $\boldsymbol{d}^{vc}$ perpendicular to the QW plane (Z-excitons). Taking $L_w = 60$ Å, $L_b = 40$ Å, we plot τ_L and τ_Z as functions of k for $\varepsilon_b = 6$, $\tilde{\varepsilon} = 4 + 3$i and $\varepsilon_b = 4$, $\tilde{\varepsilon} = 6 + 3$i in figures 10(a) and 10(b). It is seen from the plot that the lifetime does not depend drastically on the polarization and the real parts of the dielectric constants. Figure 11 shows that the dependence on L_w is also weak, while L_b (figure 12), when it grows, gives an obvious exponential factor (clearly seen from the hyperbolic functions in the denominators of (74), (75)). The most interesting dependence is that on k. We see that τ exhibits a minimum at $k_{min} \sim 1/L_b$. This dependence may be easily understood if one recalls that the dipole–dipole interaction between two planes behaves like

$$V(\boldsymbol{k}, z) \sim k\mathrm{e}^{-kz} \tag{78}$$

which, when substituted into the Fermi Golden Rule gives the correct asymptotics $\tau \sim 1/k$ at $k \to 0$ and exponential growth at $k \to \infty$.

Typical values of k for the quasi-thermalized exciton distribution with temperature $\sim$ 100 K are $\sim 3 \times 10^6$ cm^{-1}. We see that the corresponding lifetimes (tens of picoseconds) are much less than the exciton recombination rate which is about 100–200 ps in II–VI semiconductor QWs, as reported by different authors ([7] and references therein, [37]). Thus, the dipole–dipole transfer mechanism, considered above, proves to be efficient enough to transfer a large fraction of the semiconductor excitation energy to the organic medium. Moreover, the intraband relaxation of excitons due to the acoustic phonon scattering occurs on timescales of the order of 20–30 ps at 10 K [37], which is larger than the minimal transfer lifetime, obtained here (less than 10 ps for $k_{min} \sim 10^6$ cm^{-1}). This makes it reasonable to excite the QW in such a way as to produce the initial nonequilibrium distribution of excitons with $k = k_{min}$, tuning the frequency of the excitation pulse to exceed the energy

$E_{exc}(k_{min})$ of the exciton with $k = k_{min}$ by one LO-phonon frequency Ω_{LO} (since in II–VI semiconductors the free-carrier-to-exciton relaxation is governed mainly by LO-phonon scattering and happens in times of about 1 ps [37–40]), or an integer multiple of Ω_{LO}, if the exciton binding energy is larger than $\hbar\Omega_{LO}$. A numerical estimate for ZnSe gives $E_{exc}(k_{min}) - E_{exc}(k = 0) \sim 1$ meV, while $\hbar\Omega_{LO} \approx 31$ meV [37], so the kinetics of excitons at $k \sim k_{min}$ is governed mainly by the acoustic phonons.

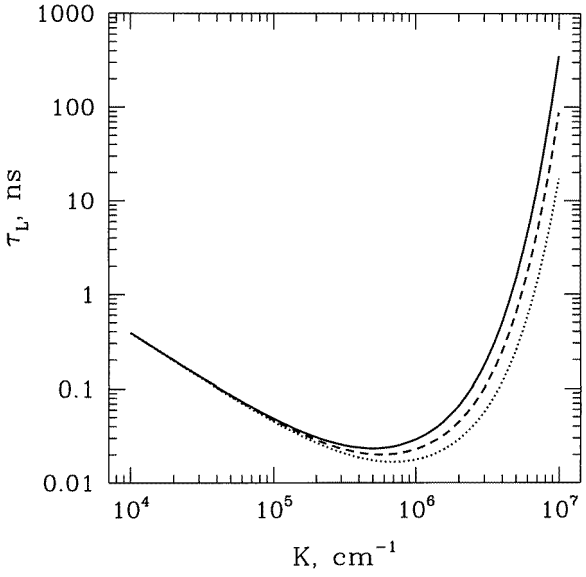

Figure 13. As figure 11, but for the III–V semiconductor compounds ($\varepsilon_b \approx 11$, $d^{vc} \approx 0.05ea_B$, all other parameters being the same as in figure 11).

Analogous calculations may be performed for the case of III–V semiconductor materials. We take $\varepsilon_b \approx 11$, $d^{vc} \approx 0.05ea_B$ and plot the L-exciton lifetime versus the wavevector k for several values of L_w (figure 13, analogous to figure 10 for II–VI materials). All of the other parameters are the same as in figure 10. We see that the lifetime is longer than that in figure 10 by about an order of magnitude, which is due to the larger values of a_B and ε_b. However, the exciton recombination time in III–V materials is also larger (0.5–1 ns [41]), so the energy transfer discussed here is still efficient enough.

3.2. Localized excitons

Now we turn to the situation in which the QW width fluctuations and the alloy disorder localize the wavefunction of the centre-of-mass exciton motion. If we denote it by $\Phi(\boldsymbol{r}_\parallel)$, which is no longer just a plane wave, the corresponding polarization is given by

$$\boldsymbol{P}(\boldsymbol{r}) = \boldsymbol{d}^{vc}\sqrt{\frac{2}{\pi a_B^2}}\frac{2}{L_w}\cos^2\left(\frac{\pi z}{L_w}\right)\Phi(\boldsymbol{r}_\parallel) \tag{79}$$

which implies that $\Phi(\boldsymbol{r}_\parallel)$ is normalized according to

$$\int \mathrm{d}^2\boldsymbol{r}_\parallel \; |\Phi(\boldsymbol{r}_\parallel)|^2 = 1. \tag{80}$$

The solution of the Schrödinger equation for a particle in the random potential, caused by the QW width fluctuations and the alloy disorder, is beyond the scope of the present paper (much work has been done in this field; e.g. see [42] and references therein). We can only state some general properties that $\Phi(\boldsymbol{r}_\parallel)$ should have: (i) it should be localized within some distance $L \gtrsim L_w$ and as it corresponds to a ground state in some potential well; (ii) it should be smooth and without nodes. As a consequence, its spatial Fourier expansion should contain mainly the components with wavevectors $k \lesssim 1/L$.

Expanding the wavefunction $\Phi(\boldsymbol{r}_\parallel)$, the charge density $\rho(\boldsymbol{r})$ and the potential $\varphi(\boldsymbol{r})$ into plane waves

$$\begin{aligned}\Phi(\boldsymbol{r}_\parallel) &= \int \frac{\mathrm{d}^2\boldsymbol{k}}{(2\pi)^2}\ \Phi_{\boldsymbol{k}} \mathrm{e}^{\mathrm{i}\boldsymbol{k}\cdot\boldsymbol{r}_\parallel} \\ \rho(\boldsymbol{r}_\parallel) &= \int \frac{\mathrm{d}^2\boldsymbol{k}}{(2\pi)^2}\ \rho_{\boldsymbol{k}}(z) \mathrm{e}^{\mathrm{i}\boldsymbol{k}\cdot\boldsymbol{r}_\parallel} \\ \varphi(\boldsymbol{r}) &= \int \frac{\mathrm{d}^2\boldsymbol{k}}{(2\pi)^2}\ \varphi_{\boldsymbol{k}}(z) \mathrm{e}^{\mathrm{i}\boldsymbol{k}\cdot\boldsymbol{r}_\parallel}\end{aligned} \tag{81}$$

we again obtain equation (69), but the charge density is given by

$$\rho_{\boldsymbol{k}}^{(X)}(z) = \mathrm{i}k_x L_w \tilde{\rho}_0 L \Phi_{\boldsymbol{k}}(1 + \cos qz) \tag{82}$$

$$\rho_{\boldsymbol{k}}^{(Z)}(z) = -q L_w \tilde{\rho}_0 L \Phi_{\boldsymbol{k}} \sin qz \tag{83}$$

$$\tilde{\rho}_0 = \sqrt{\frac{2}{\pi a_B^2}} \frac{d^{vc}}{L L_w^2}. \tag{84}$$

The solution is

$$\varphi_{\boldsymbol{k}}(z) = \tilde{\rho}_0 L \Phi_{\boldsymbol{k}} C_{\boldsymbol{k}} \mathrm{e}^{-k(z - L_b - L_w/2)} \tag{85}$$

with the same $C_{\boldsymbol{k}}$, given by (74), (75). For the decay rate we obtain

$$\frac{1}{\tau} = \frac{\operatorname{Im}\tilde{\varepsilon}}{2\pi\hbar} \int_{L_b + L_w/2}^{+\infty} \mathrm{d}z \int \frac{\mathrm{d}^2\boldsymbol{k}}{(2\pi)^2}\ 2k^2 |\varphi_{\boldsymbol{k}}(z)|^2 \tag{86}$$

from which

$$\frac{1}{\tau} = \frac{\operatorname{Im}\tilde{\varepsilon}}{\pi^2\hbar} \frac{|d^{vc}|^2}{a_B^2} \frac{1}{L_w^4} \int \frac{\mathrm{d}^2\boldsymbol{k}}{(2\pi)^2}\ k |\Phi_{\boldsymbol{k}}|^2 |C_{\boldsymbol{k}}|^2. \tag{87}$$

It is possible to get some information about the decay rate (86) based only on general properties of the wavefunction, mentioned above. We have three length scales in our problem: L_w, L_b and L. First, we have the condition $L_w \lesssim L$. Since wavevectors with $kL \gtrsim 1$, being cut off by $|\Phi_{\boldsymbol{k}}|^2$, do not contribute to the integral, we may set $kL_w \to 0$. The subsequent analysis depends on the relation between L_b and L.

If $L_b \ll L$, we may put $kL_b \to 0$ as well. Then we have

$$\frac{C_{\boldsymbol{k}}^{(X)}}{L_w^2} \longrightarrow -\frac{2\pi\mathrm{i}}{\tilde{\varepsilon}} \frac{k_x}{k} \qquad \frac{C_{\boldsymbol{k}}^{(Z)}}{L_w^2} \longrightarrow \frac{2\pi}{\varepsilon_b} \tag{88}$$

and the integral may be estimated as

$$\frac{1}{\tau_X} = A \frac{2}{\hbar} \frac{\operatorname{Im}\tilde{\varepsilon}}{|\tilde{\varepsilon}|^2} \frac{|d^{vc}|^2}{a_B^2} \frac{1}{L} \qquad \frac{1}{\tau_Z} = A \frac{4}{\hbar} \frac{\operatorname{Im}\tilde{\varepsilon}}{\varepsilon_b^2} \frac{|d^{vc}|^2}{a_B^2} \frac{1}{L} \tag{89}$$

up to a numerical factor $A \sim 1$, determined by the detailed shape of $\Phi_{\boldsymbol{k}}$. We have set the average value of k over the wavefunction $\Phi_{\boldsymbol{k}}$ to be $1/L$ and, if for the X-polarization we

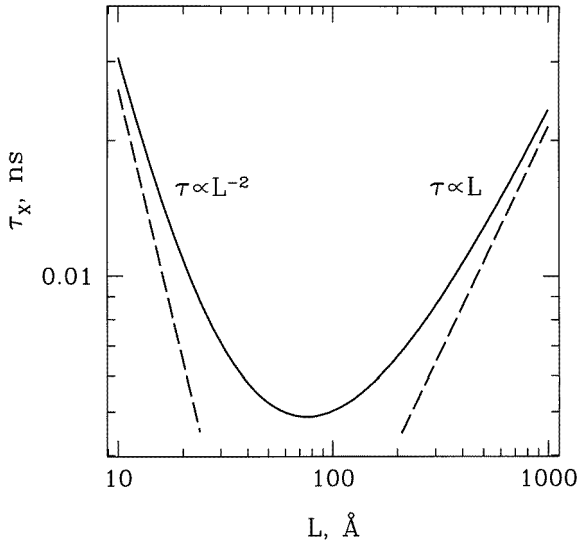

Figure 14. The localized-X-exciton lifetime τ (ns) versus the localization length L (Å) (solid line) along with the limiting cases $L \ll L_b$ and $L \gg L_b$ (dashed lines). $L_w \ll L$, $L_b = 40$ Å, $\varepsilon_b = 6$, $\tilde{\varepsilon} = 4 + 3\mathrm{i}$.

assume $\Phi_{\boldsymbol{k}}$ to be cylindrically symmetric (which may be considered as the average over the realizations of disorder), then the numerical factor is the same for both cases.

In the opposite limit, $L_b \gg L$ (which also implies $L_b \gg L_w$), we may set $\Phi_{\boldsymbol{k}} = \Phi_{\boldsymbol{k}=0}$ since the values of $\boldsymbol{k}$, contributing to the integral, are determined by $C_{\boldsymbol{k}}$ (namely, $k \lesssim 1/L_b$), which in this limit takes the form

$$\frac{C_{\boldsymbol{k}}^{(X)}}{L_w^2} \longrightarrow -\frac{\mathrm{i}k_x}{k}\frac{4\pi}{(\tilde{\varepsilon}+\varepsilon_b)\mathrm{e}^{kL_b} + (\tilde{\varepsilon}-\varepsilon_b)\mathrm{e}^{-kL_b}} \tag{90}$$

$$\frac{C_{\boldsymbol{k}}^{(Z)}}{L_w^2} \longrightarrow \frac{4\pi}{(\tilde{\varepsilon}+\varepsilon_b)\mathrm{e}^{kL_b} - (\tilde{\varepsilon}-\varepsilon_b)\mathrm{e}^{-kL_b}}. \tag{91}$$

Estimating the integral, we have

$$\frac{1}{\tau_X} = A\frac{1}{\pi\hbar}\frac{\operatorname{Im}\tilde{\varepsilon}}{|\tilde{\varepsilon}+\varepsilon_b|^2}\frac{|d^{vc}|^2}{a_B^2}\frac{|\Phi_{\boldsymbol{k}=0}|^2}{L_b^3} \tag{92}$$

where $|\Phi_{\boldsymbol{k}=0}|^2 \sim L^2$, which follows from the normalization condition. The expression for $1/\tau_Z$ differs from this by an additional factor of 2 and the factor A may be different in the two cases. It is determined by the values of $\tilde{\varepsilon}$, ε_b and is bounded by

$$A = \int_0^\infty \frac{\xi^2\,\mathrm{d}\xi}{|(\varepsilon_b/|\varepsilon_b+\tilde{\varepsilon}|)\sinh\xi + (\tilde{\varepsilon}/|\varepsilon_b+\tilde{\varepsilon}|)\cosh\xi|^2} \tag{93}$$

$$\frac{\pi^2}{12} = \int_0^\infty \frac{\xi^2\,\mathrm{d}\xi}{\cosh^2\xi} < A < \int_0^\infty \frac{\xi^2\,\mathrm{d}\xi}{\sinh^2\xi} = \frac{\pi^2}{6}. \tag{94}$$

So we see that at $L \ll L_b$ the decay rate is proportional to L^2, while at $L \gg L_b$ it is proportional to L^{-1}; therefore it has a maximum at some $L \sim L_b$. This is in agreement with the results of the previous section, since the plane waves, giving the largest contribution to the wavefunction $\Phi(\boldsymbol{r}_\parallel)$ and thus determining the decay rate, have values of the wavevector

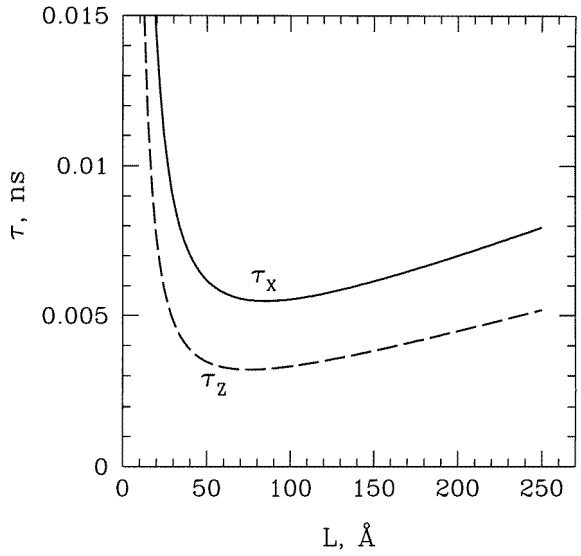

Figure 15. Localized-X-exciton (solid line) and localized-Z-exciton (dashed line) lifetimes τ (ns) versus the localization length L (Å). $L_w = 10$ Å, $L_b = 40$ Å, $\varepsilon_b = 6$, $\tilde{\varepsilon} = 4 + 3\mathrm{i}$.

of the order of $k \sim 1/L$ and we have seen that the wavevectors corresponding to the shortest lifetimes were $k_{min} \sim 1/L_b$.

To illustrate these considerations, we choose a specific example of the localized wavefunction—that of the ground state in the isotropic parabolic potential:

$$\Phi_k = \sqrt{4\pi} L \mathrm{e}^{-k^2 L^2/2} \tag{95}$$

which obviously has all of the necessary features mentioned at the beginning of this section. For this wavefunction the integral in (86) may be evaluated numerically for arbitrary parameters L, L_w, L_b (we recall that the only physically relevant ones are $L \gtrsim L_w$). The results of the calculation (τ versus L) are plotted in figures 14, 15 along with the asymptotic dependencies for $L_b = 40$ Å, $\varepsilon_b = 6$, $\tilde{\varepsilon} = 4 + 3\mathrm{i}$ (we have set $L_w \to 0$ for the plots in figure 14, but a more specific value $L_w = 10$ Å was chosen for figure 15). In the limit $L \gg L_b$, the coefficient A is $\sqrt{\pi}/2$, while for $L \ll L_b$, A was calculated numerically, as given by (93).

We also plot the dependence, analogous to that in figure 15, for parameters typical of III–V semiconductors: $d^{vc}/ea_B = 0.05$ and $\varepsilon_b = 11$ (figure 16); analogously to the previous section, we obtain larger lifetimes than those for II–VI semiconductors.

Calculations analogous to those for free and localized excitons may also be performed for the case in which populations of free electrons and holes rather than bound excitons are present. First, the decay rate of a single free electron–hole pair is determined from equation (65), starting from the wavefunction being the direct product of two 2D plane waves. Then the expression obtained has to be averaged over the proper momentum distributions for electrons and holes. This was done in the approximation of an ideal quasi-equilibrium Fermi gas, and the dipole–dipole lifetimes obtained turn out to be as long as 300 ps (and larger) for II–VI semiconductors and about an order of magnitude larger for III–V semiconductors.

Summarizing the results of this section, we can say that the kinetics of the initial free-

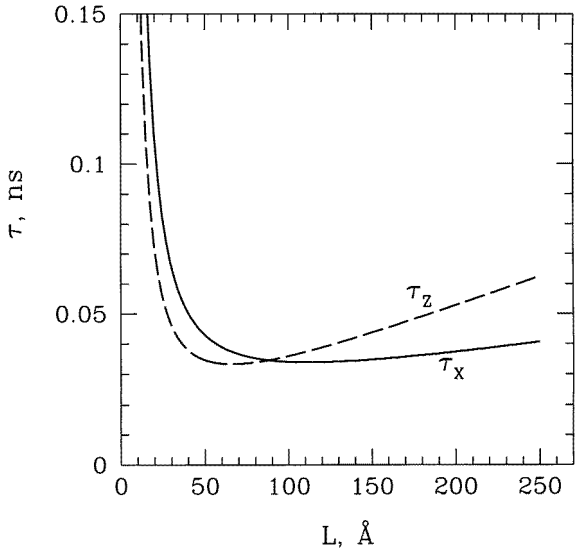

Figure 16. As figure 15, but for the III–V semiconductor compounds, other parameters being the same as for figure 15.

carrier population (produced, e.g., by the electrical pumping) is not significantly changed by the presence of the organic medium, since the energy transfer from free carriers turns out to be slower than the process of exciton formation ($\sim$1 ps). On the other hand, the subsequent evolution of bound excitons is strongly affected by the presence of the organic medium. In an isolated QW, excitons recombine for several hundred ps. In contrast to this, excitons coupled to the organic medium efficiently transfer the larger part of their energy to the organic molecules before they recombine inside the QW. For quantum wells, based on the II–VI semiconductors and in a realistic geometry, such transfer may occur on timescales of the order of 10 ps. This simple physical picture shows that the system studied here may be promising for optical devices based on hybrid organic–inorganic structures, combining good transport properties of semiconductors and large oscillator strengths characteristic of organic materials to achieve efficient electroluminescence.

4. Conclusions

The method of OMBD combined with a careful substrate preparation and sample characterization has been successful in growing layered systems including organic crystalline materials (e.g., tetracene, perylene, fullerene, PTCDA). There is little doubt that in the future the number of molecular species used will rapidly increase and that a large flexibility in the design of novel types of structure will be achieved. In particular, hybrid multilayer systems containing layers of organic and inorganic materials are widely used in different optical devices [3]. However, the situation studied in this review, namely, that in which excitons in OQW and IQW are resonant, is especially interesting, since it leads to several types of new phenomenon.

We have discussed the linear and nonlinear optical properties of novel hybrid excitons in organic–inorganic heterostructures. With respect to those of the usual semiconductor quantum wells, a very strong enhancement of both the linear and nonlinear parts of the

susceptibility is predicted. These results are rationalized in terms of the large oscillator strength of Frenkel excitons and the low saturation density of Wannier excitons: these two characteristics are exhibited by the hybrid resonances simultaneously. If successfully synthesized, structures of the type considered here would exhibit pronounced nonlinearities of potential technological interest. Moreover, the hybrid excitons are a promising system as regards possible novel electro-optical and magneto-optical properties. We have also shown that, due to the parity breaking in the hybrid organic–inorganic structure, second-order nonlinearity is present, and thus there exists the possibility of second-harmonic generation. We have also considered the new possibilities which may appear for microcavities containing resonating organic and inorganic QWs. In such structures we can expect a drastic reduction of the relaxation time of excitons to produce states having a large radiative width and a short fluorescence decay time.

The case of strongly broadened excitonic resonances in the organic material was also considered. In this case the resonant dipole–dipole coupling leads to efficient Förster energy transfer from the IQW to the organic medium. We can also expect that the combination of electrical pumping of excitons in inorganic QWs with the fast relaxation and fluorescence of excitons in organics will open up a new scenario of excitonic processes, of interest for both basic science and device applications.

More detailed theoretical calculations are needed, but probably the crucial factor will be the technological progress in the synthesis of such structures. We believe that this is a very promising field of research and hope that the experimental efforts to grow and investigate these novel systems will be successful.

Acknowledgments

It is a pleasure to thank N Bloembergen for a stimulating discussion on the issue of SHG in hybrid heterostructures. Partial support from INFM through the project ‘Photoactive Organic Materials’ (PAIS G) is acknowledged. VMA is grateful to the Scuola Normale Superiore (Pisa, Italy) for hospitality and support. He also acknowledges partial support through Grant 96-0334049 from the Russian Foundation of Basic Research, a Grant from ‘Physics of Nanostructures’, the Russian Ministry of Science and Technology, and INTAS Grant 93-461.

References

[1] Rashba E I and Sturge M D (ed) 1982 *Excitons* (Amsterdam: North-Holland)
[2] Green B I, Orenstein J and Schmitt-Rink S 1990 *Science* **247** 679
[3] Forrest S R 1997 *Chem. Rev.* **97** 1793
[4] Agranovich V M, Atanasov R and Bassani F 1994 *Solid State Commun.* **92** 295
[5] Bastard G 1988 *Wave Mechanics Applied to Semiconductor Heterostructures* (Paris: CNRS)
[6] Atanasov R, Bassani F and Agranovich V M 1994 *Phys. Rev.* B **49** 2658
[7] Cingolani R 1997 *Semiconductors and Semimetals* vol 44 (New York: Academic) pp 163–226
[8] Yamada T, Hoshi H, Manaka T, Ishikawa K, Takezoe H and Fukuda A 1996 *Phys. Rev.* B **53** R13 314
[9] Hebard A F, Haddon R C, Fleming R M and Kortan A R 1991 *Appl. Phys. Lett.* **59** 2109
[10] Kohl M, Heitmann D, Grambow P and Ploog K 1990 *Phys. Rev.* B **42** 2941
[11] La Rocca G C 1996 *Phys. Scr.* T **66** 142
[12] *Landolt–Börnstein New Series* 1987 Group III, vol 22a, ed O Madelung (Berlin: Springer)
[13] Schmitt-Rink S, Chemla D S and Miller D A B 1985 *Phys. Rev.* B **32** 6601
Schmitt-Rink S, Chemla D S and Miller D A B 1989 *Adv. Phys.* **38** 89
[14] Jaziri S, Romdhane S, Bouchriha H and Bennaceur R 1997 *Phys. Lett.* **234A** 141
[15] Schultheis L, Honold A, Kuhl J, Köhler K and Tu C W 1986 *Phys. Rev.* B **34** 9027

[16] Vinattieri A, Shah J, Damen T C, Kim D S, Pfeiffer L N and Sham L J 1993 *Solid State Commun.* **88** 189
[17] Orrit M, Bernard J, Turlet J M and Kottis P 1983 *J. Chem. Phys.* **78** 2847
[18] D'Andrea A and Muzi R 1995 *Solid State Commun.* **95** 493
[19] La Rocca G C, Bassani F and Agranovich V M 1996 *Notions and Perspectives of Nonlinear Optics* ed O Keller (Singapore: World Scientific)
La Rocca G C, Bassani F and Agranovich V M 1995 *Nuovo Cimento* D **17** 1555
[20] Haug H and Koch S W 1994 *Quantum Theory of the Optical and Electronic Properties of Semiconductors* 3rd edn (Singapore: World Scientific)
[21] Honold A, Schultheis L, Kuhl J and Tu C W 1989 *Phys. Rev.* B **40** 6442
Deveaud B, Clérot F, Roy N, Satzke K, Sermage B and Katzer D S 1991 *Phys. Rev. Lett.* **67** 2355
[22] La Rocca G C and Bassani F 1998 *Phys. Lett.* **A** at press
[23] Atanasov R, Bassani F and Agranovich V M 1994 *Phys. Rev.* B **50** 7809
[24] Bloembergen N, Chang R K, Jha S S and Lee C H 1968 *Phys. Rev.* **174** 813
[25] Agranovich V M and Ginzburg V L 1984 *Crystal Optics with Spatial Dispersion and Excitons* (Berlin: Springer)
[26] Yudson V I, Reineker P and Agranovich V M 1995 *Phys. Rev.* B **52** R5543
[27] Engelmann A, Yudson V I and Reineker P 1998 *Phys. Rev.* B **57** 1784
[28] Agranovich V, Benisty H and Weisbuch C 1997 *Solid State Commun.* **102** 631
[29] Burstein E and Weisbuch C (ed) 1995 *Confined Electrons and Photons: New Physics and Applications* (New York: Plenum)
[30] Zhang Bei, Zhuang Lei, Lin Yong, Xia Zhongju, Ma Yong, Ding Xiamin, Wang Shumin, Zhou Dejian and Huang Chunhui 1996 *Solid State Commun.* **87** 445
Dodabalapur A, Rothery L J, Miller T M and Kwoch E W 1994 *Appl. Phys. Lett.* **64** 2486
Takada N, Tsutsui T and Saito S 1993 *Appl. Phys. Lett.* **63** 2032
[31] Vaubel G and Baessler H 1970 *Mol. Cryst. Liq. Cryst.* **12** 39
Turlet J M and Philpott M R 1975 *J. Chem. Phys.* **62** 4260
[32] Lidzey D G, Bradley D D C, Skolnick M S, Virgili T, Walker S and Whittaker D M 1998 *Nature* at press
[33] Tassone F, Piermarocchi C, Savona V, Quattropani A and Schwendimann P 1997 *Phys. Rev.* B **56** 7554
[34] Agranovich V M, La Rocca G C and Bassani F 1997 *JETP Lett.* **66** 748
[35] Basko D M, La Rocca G C, Bassani F and Agranovich V M 1998 *Eur. Phys. J.* B submitted
[36] A similar idea has been used to calculate the energy transfer from an excited dye molecule to the surrounding solution, considering the molecule as a point classical dipole and the solution as a continuous absorbing medium:
Galanin M D and Frank I M 1951 *Zh. Eksp. Teor. Fiz.* **21** 114
Galanin M D 1951 *Zh. Eksp. Teor. Fiz.* **21** 126
[37] Umlauff M, Hoffmann J, Kalt H, Langbein W, Hvam J M, Scholl M, Söllner J, Henken M, Jobst B and Hommel D 1998 *Phys. Rev.* B **57** 1390
[38] Permogorov S 1975 *Phys. Status Solidi* b **68** 9
[39] Permogorov S and Travnikov V 1979 *Solid State Commun.* **29** 615
[40] Pelekanos N, Ding J, Fu Q, Nurmikko A V, Durbin S M, Kobayashi M and Gunshor R L 1991 *Phys. Rev.* B **43** 9354
[41] Shah J 1996 *Ultrafast Spectroscopy of Semiconductors and Semiconductor Nanostructures* (Berlin: Springer)
[42] Zimmerman R 1997 *Pure Appl. Chem.* **69** 1179